# Violet-light suppression of thermogenesis by Opsin 5 hypothalamic neurons

**Kevin X. Zhang**[1,2,7,8], **Shane D'Souza**[1,2,7], **Brian A. Upton**[1,2,7,8], **Stace Kernodle**[11], **Shruti Vemaraju**[1,2], **Gowri Nayak**[1,2], **Kevin D. Gaitonde**[1,2,7,8], **Amanda L. Holt**[13], **Courtney D. Linne**[1,2,7,8], **April N. Smith**[1,2], **Nathan T. Petts**[5], **Matthew Batie**[5], **Rajib Mukherjee**[4], **Durgesh Tiwari**[6], **Ethan D. Buhr**[14], **Russell N. Van Gelder**[14,15,16], **Christina Gross**[6,10], **Alison Sweeney**[13], **Joan Sanchez-Gurmaches**[3,4,10], **Randy J. Seeley**[11,12], **Richard A. Lang**[1,2,3,9,*]

[1]The Visual Systems Group, Abrahamson Pediatric Eye Institute, Cincinnati Children's Hospital Medical Center, Cincinnati, OH 45229, USA

[2]Center for Chronobiology, Divisions of Pediatric Ophthalmology, Cincinnati Children's Hospital Medical Center, Cincinnati, OH 45229, USA

[3]Developmental Biology, Cincinnati Children's Hospital Medical Center, Cincinnati, OH 45229, USA

[4]Endocrinology, Cincinnati Children's Hospital Medical Center, Cincinnati, OH 45229, USA

[5]Clinical Engineering, Cincinnati Children's Hospital Medical Center, Cincinnati, OH 45229, USA

[6]Neurology, Cincinnati Children's Hospital Medical Center, Cincinnati, OH 45229, USA

[7]Molecular and Developmental Biology Graduate Program, College of Medicine, Cincinnati, OH 45229, USA

[8]Medical Scientist Training Program, University of Cincinnati, College of Medicine, Cincinnati, OH 45229, USA

[9]Department of Ophthalmology, University of Cincinnati, College of Medicine, Cincinnati, OH 45229, USA

[10]Department of Pediatrics, University of Cincinnati, College of Medicine, Cincinnati, OH 45229, USA

[*]Corresponding author: **Richard A. Lang**, Division of Pediatric Ophthalmology, Cincinnati Children's Hospital Medical Center, 3333 Burnet Avenue, Cincinnati, OH 45229, Tel: 513-636-2700 (Office), 513-803-2230 (Assistant), Fax: 513-636-4317. Richard.Lang@cchmc.org.

[11]Department of Surgery, University of Michigan, School of Public Health, Ann Arbor, MI 48109, USA

[12]Department of Internal Medicine, University of Michigan, School of Public Health, Ann Arbor, MI 48109, USA

[13]Department of Physics, Yale University, New Haven, CT 06520

[14]Department of Ophthalmology, University of Washington Medical School, Seattle, WA 98104, USA

[15]Department of Biological Structure, University of Washington Medical School, Seattle, WA 98104, USA

[16]Department of Pathology, University of Washington Medical School, Seattle, WA 98104, USA

## Abstract

The opsin family of G-protein coupled receptors are employed as light detectors in animals. Opsin 5 (neuropsin, OPN5) is a highly conserved, violet light (380 nm $\lambda_{max}$) sensitive opsin[1,2]. In mice, OPN5 is a known photoreceptor in retina[3] and skin[4] but is also expressed in the hypothalamic preoptic area (POA)[5]. Here we describe a light-sensing pathway in which *Opn5* expressing POA neurons regulate brown adipose tissue (BAT) thermogenesis. We show *Opn5* expression in glutamatergic warm-sensing POA neurons that receive synaptic input from multiple thermoregulatory nuclei. We further show that *Opn5* POA neurons project to BAT and decrease its activity under chemogenetic stimulation. *Opn5* null mice show overactive BAT, elevated body temperature, and exaggerated thermogenesis when cold challenged. Moreover, violet photostimulation during cold exposure acutely suppresses BAT temperature in wild-type, but not in *Opn5* null mice. Direct measurements of intracellular cAMP *ex vivo* reveal that *Opn5* POA neurons increase cAMP when stimulated with violet light. This analysis thus identifies a violet light sensitive deep brain photoreceptor that normally suppresses BAT thermogenesis.

The availability of photons emanating from our sun has been exploited for adaptive advantage by almost all living systems. For example, the visual sense of animals relies on detection of radiant photons for object identification. Plants and animals also anticipate the daily light-dark cycle using non-visual pathways to entrain circadian clocks. In animals, both visual and non-visual pathways employ the eyes for photic input, but extraocular light detection has been well-described in non-mammalian species. For example, in the fruit fly and in zebrafish, light can entrain the circadian clock in organs directly, without the need for input from the eyes[6]. Though it had been thought that mammals do not employ extraocular light detection, this view has recently changed[4,7–9].

In animals, most light response pathways employ a member of the opsin family of G-protein coupled receptors as a light detector. Of the non-visual opsins, melanopsin (OPN4), a blue light sensitive (480 nm $\lambda_{max}$) opsin, has been most extensively studied in mice: ocular melanopsin has a role in circadian entrainment[10], the pupillary light reflex[11], eye development[12] as well as mood and learning[13]. Recently, studies of the visual violet light sensitive (380 nm $\lambda_{max}$)[1,2] neuropsin (OPN5) and blue light sensitive encephalopsin (OPN3) have provided evidence for their involvement in extraocular light response pathways. In

birds, *Opn5* expression in the brain is implicated in the regulation of seasonal breeding behavior[14] and in mice is necessary and sufficient for direct photoentrainment of retinal, corneal, and skin circadian clocks[3,4]. OPN3 was recently shown to be expressed in adipocytes where it promotes lipolysis in a blue light-dependent manner[7,15].

In the mouse and primate hypothalamus, *Opn5* is expressed in the preoptic area (POA)[5] and this raised the possibility that, as in birds, OPN5 might function as a deep brain photosensor. The POA is a thermoregulatory region that in mouse modulates the heat-generating capacity of brown adipose tissue (BAT) via sympathetic nervous system activity (SNS)[16]. Homeotherms rely on this system to defend core body temperature against ever-changing environments. This hypothalamic-BAT neuraxis has been extensively described[17]. Here, we provide evidence that the thermoregulatory apparatus of mice is violet light responsive in an OPN5-dependent manner. We further show that the crucial light sensitive cells are neurons that reside in the preoptic area of the hypothalamus.

## *Opsin 5* in POA thermoregulatory neurons

Using an *Opn5*<sup>*cre*</sup> knock-in allele to activate the tdTomato reporter *Ai14* (*Opn5*<sup>*cre/+*</sup>; *Ai14* mice), we identified *Opn5* expression in the preoptic area (POA) of the hypothalamus in postnatal day (P)21 mice (Fig. 1a, b). We confirmed that this region was actively transcribing *Opn5* using Xgal labeling in brain tissue from P10 *Opn5*<sup>*lacZ/+*</sup> mice (Fig. 1c, d). Ai14+ neurons were also found in the raphe pallidus (Extended Data Fig. 1a–c) but were Xgal negative in P12 *Opn5*<sup>*lacZ/+*</sup> cryosections (Extended Data Fig. 1d), suggesting *Opn5*<sup>*cre/+*</sup>; *Ai14* lineage marking from an earlier developmental stage. A comprehensive lineage survey outside the CNS revealed no *Opn5* expression in brown and white adipose tissue, thyroid, liver, heart, adrenal, and pancreas (Extended Data Fig. 1e–k).

The POA contains several discrete neuronal subtypes associated with homeostatic control. We used multiplex fluorescence *in situ* hybridization (M-FISH) to label distinct subpopulations in the POA of P21 *Opn5*<sup>*cre/+*</sup>; *Ai14* mice (Fig. 1e): the majority of *Opn5* POA neurons expressed *Slc17a6* (vesicular glutamate transporter 2, VGLUT2) and thus were glutamatergic, while only a small fraction colabeled with *Slc32a1* (vesicular GABA transporter, VGAT)(Fig. 1f–h). The POA also contains temperature-sensitive neurons that co-express the neuropeptides PACAP (*Adcyap1*) and BDNF (*Bdnf*)[18] and use TRPM2 as a heat sensor[19]. Using M-FISH, we found that nearly all *Opn5* POA neurons colabeled for *Adcyap1* and *Bdnf* (Fig. 1i–k) and approximately half co-express *Trpm2* (Extended Data Fig. 2a–c). Thus, *Opn5* POA neurons are BDNF+/PACAP+ warm-sensitive glutamatergic neurons.

To map presynaptic inputs to *Opn5* POA neurons, we injected a tracing rabies virus into the POA of P21 *Opn5*<sup>*cre/+*</sup>; *Ai6; RΦGT*[20] mice (Fig. 1l, m). Six days post-injection, we identified tdTomato-positive neurons in the paraventricular nucleus (PVN, Fig. 1n–p), the supraoptic nucleus (SON, Fig. 1n,o,q), the dorsomedial hypothalamus (DMH, Fig. 1r,s), the lateral parabrachial nucleus (LPB, Fig. 1t, u), and raphe pallidus (RPa, Fig. 1v,w). These regions all have a role in thermoregulation (Fig. 1x), with the DMH, LPB, and RPa directly implicated in the cutaneous thermosensory circuit that controls brown adipose tissue (BAT)

activity[17]. Taken together, these results indicate that *Opn5* POA neurons are an excitatory, warm-sensitive population synaptically connected to thermoregulatory nuclei.

## *Opn5* POA neurons regulate BAT activity

We next evaluated whether *Opn5* POA neurons communicated with BAT. We injected a transneuronal retrograde pseudorabies virus (PRV) expressing mRFP1 into the BAT of P60 *Opn5*$^{cre/+}$; *Ai6* mice (Fig. 2a). Five days post-injection, we identified mRFP1-positive neurons in the intermediolateral nucleus (IML) of the spinal cord, RPa, DMH, PVN, the nucleus tractus solitarius (NTS), and the lateral hypothalamic area (LHA)(Fig. 2b–g), all regions implicated in BAT thermogenesis. Importantly, we identified mRFP1-positive neurons in the POA that colabeled with *Ai6* (Fig. 2h, i), demonstrating that a direct polysynaptic pathway exists between *Opn5* POA neurons and the BAT.

To determine whether *Opn5* POA neurons can control BAT activity, we used chemogenetics to activate or inhibit these neurons while monitoring BAT and core temperature. Stimulatory hM3Dq or inhibitory hM4Di DREADDs (Designer Receptors Exclusively Activated by Designer Drugs) were targeted to *Opn5* POA neurons by injecting a cre-dependent AAV5 (Adeno Associated Virus) vector into *Opn5*$^{cre/+}$ mice (*Opn5*$^{+/+}$ mice were used as a control) (Fig. 2j–m). Animals were implanted with a telemetric sensor to monitor BAT and core temperature and each received an injection of the DREADD ligand clozapine N-oxide (CNO) for experimental and control studies (Fig. 2m). Animals were then sacrificed and the BAT harvested for molecular profiling of thermogenic gene expression (Extended Data Fig. 3a, b). We found that chemogenetic activation of *Opn5* POA neurons significantly suppressed BAT and core temperature (Fig. 2n, o). Cre-negative *Opn5*$^{+/+}$ animals administered either vehicle or CNO failed to show a similar effect (Fig. 2p, q). By contrast, chemogenetic inhibition of *Opn5* POA neurons augmented BAT and core temperature (Fig. 2r, s), with this effect absent in cre-negative controls (Fig. 2t, u). Subsequent studies performed on *Opn5*$^{cre/-}$ (loss of *Opn5* function) animals (Extended Data Fig. 3c–f) and animals under 4°C cold exposure (Extended Data Fig. 3g–l) showed that heterozygous *Opn5* loss of function does not change baseline BAT or core temperature (Extended data Fig. 3g–j) and that neither loss of *Opn5* nor temperature sensing alters the chemogenetic effects of *Opn5* POA neurons on BAT activity. Overall, these results demonstrate that *Opn5* POA neurons can robustly and bidirectionally regulate BAT activity.

## Elevated thermogenesis in *Opn5* null mice

To study the function of OPN5 in thermogenesis, we used a germ-line *Opn5* null mouse (*Opn5*$^{-/-}$)[21]. Immunodetection in *Opn5*$^{-/-}$ BAT showed elevated levels of uncoupling protein UCP1 (Extended Data Fig. 4a, b) and tyrosine hydroxylase (TH), a marker for SNS innervation (Extended Data Fig. 4c–e). Cold exposure revealed that that *Opn5*$^{-/-}$ animals were better at defending their body temperature and showed elevated thermogenesis pathway genes (Extended Data Fig. 4f, g). Telemetry sensor recording further indicted that core and BAT temperature were elevated in *Opn5* null mice even at 24°C ambient, and that these differences were not due to a dysregulated circadian rhythm (Extended Data Fig. 4h, i). By infrared thermography, cold exposed P8 and P90 *Opn5*$^{-/-}$ were warmer than controls

(Extended Data Fig. 4j, k). Surface temperatures in the Interscapular adipose (iAT) region of P90 $Opn5^{-/-}$ animals (Extended Data Fig. 4l) were quantifiably warmer, whereas tail temperatures were indistinguishable (Extended Data Fig. 4m). In aggregate, these data suggested that mice lacking $Opn5$ exhibit increased BAT thermogenesis.

The exaggerated thermogenesis of $Opn5^{-/-}$ mice does not lead to changes in body weight and composition or locomotor activity but does result in elevated energy expenditure (Extended Data Fig. 5a–f). Lack of body composition differences may be explained by the increased food and water consumption of $Opn5^{-/-}$ mice (Extended Data Fig. 5g, h). Serum lipids are lower in the $Opn5$ null, but serum thyroxine (T4) and thyrotropin-releasing hormone (TRH) are unchanged (Extended Data Fig. 6a–f), suggesting that facultative and not obligatory thermogenesis is primarily affected. Major white adipose depots are smaller in $Opn5^{-/-}$ mice, and show decreased adipocyte size and increased UCP1 (Extended Data Fig. 6g–i). Systolic and diastolic blood pressure, mean arterial pressure (MAP), and pulse rate are not different between $Opn5^{-/-}$ and $Opn5^{+/+}$ mice (Extended Data Fig. 6j–l). However, $Opn5^{-/-}$ mice show an augmented response to the β3-adrenergic agonist CL-316,243 (Extended Data Fig. 6m). These results indicate that the exaggerated BAT thermogenesis of $Opn5^{-/-}$ animals cannot be attributed to differences in thyroid hormone or cardiovascular activity, but rather, is explained by adaptive changes in adrenergic BAT sensitivity and lipid mobilization. A POA-specific $Opn5$ deletion was generated using $Lepr^{cre}$ (Extended Data Fig. 4n, o, 7a–g). We repeated the previous analyses on control ($Opn5^{fl/fl}$) and conditional mutant mice ($Lepr^{cre/+}; Opn5^{fl/fl}$) mice and found that mutant mice largely phenocopied the global $Opn5$ loss-of-function model (Extended Data Fig. 4p–v). These data provide strong support for a BAT thermogenic-suppressive role of preoptic OPN5.

## Violet light suppresses BAT activity

The observation that $Opn5^{-/-}$ mice show an exaggerated thermogenic response suggested that OPN5 normally inhibits thermogenesis. To assess whether this suppressive role depends on the light-sensing function of OPN5, we monitored BAT and core temperature in cold-exposed P90–120 $Opn5^{+/+}$ and $Opn5^{-/-}$ animals while providing acute 380 nm violet light stimulation. In $Opn5^{+/+}$ mice, violet photostimulation decreased BAT and core temperatures, whereas $Opn5^{-/-}$ mice failed to respond (Fig. 3a, b). When violet light was not supplemented, there was no longer any divergence in BAT and core temperature between $Opn5^{+/+}$ and $Opn5^{-/-}$ mice (Fig. 3c, d). To assess the possibility that the addition of violet light might invoke a differential behavioral response in $Opn5^{+/+}$ and $Opn5^{-/-}$ animals, locomotor activity was recorded and revealed no differences in average speed or distance traveled (Extended Data Fig. 8a–i).

$Opn5$ is expressed in retinal ganglion cells and can photoentrain a retinal circadian clock[3]. We utilized two approaches to assess the possibility that retinal OPN5 might contribute to changes in BAT thermogenesis. First, we conditionally deleted $Opn5^{fl}$ from retinal progenitors using $Rx^{cre}$, and found no differences in core temperature between cold exposed wild-type ($Opn5^{fl/fl}$) and retinal $Opn5$ conditional ($Rx^{cre}; Opn5^{fl/fl}$) animals (Fig. 3e). Second, we enucleated P90–120 $Opn5^{+/+}$ and $Opn5^{-/-}$ mice and subjected them to the same

cold-exposure photostimulation assay as sighted mice. Enculeated $Opn5^{+/+}$ mice decreased their core temperature in response to violet light while enucleated $Opn5^{-/-}$ showed no such response (Fig. 3f, g). Molecular profiling of dissected BAT from enucleated $Opn5^{+/+}$ and $Opn5^{-/-}$ animals showed differences in thermogenic gene induction (Fig. 3h) that resembled changes observed in sighted mice. These data show that the inhibitory role of OPN5 on BAT thermogenesis does not require retinal OPN5.

## Violet light absence enhances BAT activity

As an extension of our acute response analysis, we asked whether chronic elimination of violet photons would mimic $Opn5$ loss-of-function in wild-type mice. Male and female wild-type mice on a C57BL6/J background were raised under "full spectrum" (380 nm + 480 nm + 660 nm) or "minus violet" (480 nm + 660 nm) lighting from embryonic day (E)16.5 to P70 under a standard 12L:12D light cycle (Extended Data Fig. 9a, b). Analysis at P70 (Extended Data Fig. 9c–m) revealed that minus violet mice showed a milder version of the exaggerated thermogenesis phenotype characteristic of the $Opn5$ null.

Since our aggregated data suggested that $Opn5$ POA neurons might be directly light responsive, we assessed whether the POA received sufficient photon flux for opsin activation. Using a custom-designed optic fiber probe, we performed intra-tissue radiometry at various depths in the brain of anesthetized mice (Extended Data Fig. 10a–c). At the $\lambda_{max}$ of the OPN5 action spectrum, we measured approximately 2.5 log-fold intensity attenuation relative to the cranial surface at the depth of the POA (Extended Data Fig. 10d, e). When extrapolating for normal sunlight intensities, a maximum violet flux of $9.0 \times 10^{12}$ photons $cm^{-2}s^{-1}$ can reach the POA. This is above the activation threshold for other mammalian nonvisual opsins[22].

## OPN5 POA neurons respond to violet light

Our findings raised the crucial question of how $Opn5$ POA neurons signal in response to violet light. To gain insight into these mechanisms, we monitored real-time intracellular cyclic AMP (cAMP) using a genetically encoding a TEpacVV cAMP sensor activated transcriptionally with $Opn5^{cre}$. TEpacVV reports cAMP binding by changes in fluorescence resonance energy transfer (FRET) between an mTurquoise donor (CFP) and a Venus acceptor (cp173Venus-Venus, YFP)[23] that can be imaged using two-photon microscopy (Fig. 4a, b). Neurons that experience an elevation in intracellular cAMP, such as the response to forskolin (FK) and 3-isobutyl-1-methylxanthine (IBMX), will have an increase in the ratio of CFP to YFP ( F), while depleting cAMP by permeabilizing the cell with digitonin will decrease F (Fig. 4c–e). We designed a 1 hour experimental protocol where 15 minutes of FRET measurements in darkness were followed by 30 minutes of 50% duty cycle violet photostimulation with measurements taken in between, ending with 15 minutes of dark measurements following the application of FK + IBMX (Fig. 4f). POA slices from P21 $Opn5^{cre/+}$ animals showed a dramatic increase in relative F in response to violet photostimulation whereas slices from P21 $Opn5^{cre/-}$ animals featured little to no elevation in F and was indistinguishable from dark conditions (Fig. 4g–k). These data argue that $Opn5$

POA neurons are directly sensitive to violet photostimulation *ex vivo* and in response, increase intracellular cAMP.

## Discussion

We present evidence in mice of a violet light-sensitive thermoefferent pathway from POA to BAT that employs OPN5 (Neuropsin) as a light sensor. Acting as a deep brain photoreceptor with a peak sensitivity of 380 nm, OPN5 inhibits BAT thermogenesis through a direct light response that raises intracellular cAMP.

Deep brain photoreceptors have been extensively documented in teleost[24] and avian species[14], where nonvisual opsins regulate a host of behavioral and reproductive responses. By contrast, evidence of extraocular light sensing in mammals has only recently gained acceptance, with the precise signaling mechanisms not yet fully determined. We have previously demonstrated that adipocyte OPN3 (a blue-light sensitive opsin) increases lipolysis through promoting cAMP-dependent phosphorylation of hormone sensitive lipase and thus enhances adaptive thermogenesis in mice[7]. In this report, we use neuroanatomical and loss-of-function studies to establish preoptic area OPN5 in an inhibitory role for BAT thermogenesis. Chemogenetic stimulation of *Opn5* POA neurons immediately decreases BAT temperature, whereas mice lacking *Opn5* show profound elevations in adaptive thermogenesis and BAT activity. These opposing activities of OPN3 and OPN5 on thermogenesis raise the interesting hypothesis that nonvisual photoreceptive pathways decode light information to help calibrate time-of-day appropriate BAT activity. The precise mechanisms that integrate OPN3 and OPN5 activities in thermogenesis pathways require further study.

Recent functional studies on BDNF+/PACAP+[18], leptin receptor[25], TRPM2[19], and prostaglandin EP3 receptor[26] expressing POA neurons have uncovered evidence that glutamatergic, and not GABAergic populations, directly regulate body temperature. These data challenge prior models suggesting that BAT-projecting thermoregulatory POA neurons are GABAergic[17]. Our analysis identified *Opn5* POA neurons to be glutamatergic BDNF/PACAP double positive and, consistent with the outcome of the previous studies, showed robust decreases in BAT and core temperature under chemogenetic stimulation. Multiple lines of evidence now suggest that an excitatory subpopulation of warm-sensitive POA neurons is capable of integrating signaling from leptin, prostaglandin E2, and violet light. The most compelling evidence of this comes from a tandem scRNA-seq:MERFISH (single cell RNA-seq Multiplexed Error-Robust FISH) cell atlas of the POA, in which excitatory subcluster e13 is enriched for co-expression of *Adcyap1* (encoding PACAP), *Bdnf, Slc17a6* (encoding VGLUT2), *Ptger3* (encoding the prostogandin E2 receptor), *Lepr,* and *Opn5*[27]. It will be crucial to investigate whether this population represents a bona fide nexus for signal integration for all these pathways.

In summary, our findings have revealed an unexpected light-responsive POA-BAT neuraxis in mice that requires OPN5 as a deep brain photosensor. It will be very interesting for future work to examine the possibility that normal thermogenesis in humans requires light input via extraocular pathways. This possibility is supported by the conservation of *OPN3* expression

in human adipocytes, *OPN5* expression in the POA of primates[5], and many metabolic diseases showing a season-of-birth dependent risk[28,29], suggesting involvement of light response pathways. We speculate that insufficient stimulation of OPN3 and OPN5 in these tissues may contribute to the growing epidemic of metabolic disease in the developed world, where artificial lighting has become the norm.

## Methods

Where appropriate, statistical methods were used to predetermine sample size. With the exception of imaging analysis, investigators were not blinded to allocation during experiments and outcome assessment.

### Mice

Animals were housed in a pathogen-free vivarium maintained at an ambient temperature of 22°C and a relative humidity of 30–70%. All pharmacological and surgical procedures were conducted in accordance with protocols approved by the Institutional Animal Care and Use Committee at Cincinnati Children's Hospital Medical Center (Protocol Number 2018– 0046). This study is compliant with all relevant ethical regulations regarding animal research. Genetically modified mice used in this study include: *Rx-cre, Ai14* (Jax stock 007914), *Ai6* (Jax stock 007906), *RΦGT* (Jax stock 024708)[20], *CAMPER* (*Rapgef3* Jax Stock 032205), *Lepr-cre* (*ObRb-cre*, Jax stock 008320), and *Opn5^tm1a(KOMP)Wtsi* that were generated from C57BL/6N embryonic stem cells obtained from KOMP (embryonic stem clone ID: KOMP-HTGRS6008_A_B12-Opn5-ampicillin) as previously described[21]. Briefly, the embryonic stem cells harbor a genetic modification in which a *LacZ-Neomycin* cassette is flanked by FRT sites, between exon 3 and exon 4, and a *loxp* site separates *LacZ* from the neomycin coding region. *Loxp* sites also flank exon 4 of *Opn5*, allowing multiple mouse lines that can serve as reporter nulls, conditional floxed and null mice. The *Opn5^fl* allele was created by crossing the *Opn5^tm1a(KOMP)Wtsi* mice to *FLPeR* (Jax stock 003946) to remove the *LacZ* cassette. The *Opn5^{-/-}* line was created by crossing the *Opn5^fl* mice to *E2a-cre* (Jax stock 003724). The *Opn5^{-/-}* line was propagated under a mixed background (C57/129/CD1/ FVB). Littermate control animals were used for all experiments with the exception of C57BL/6J mice, which were reared under different lighting conditions. The *Opn5^cre* mice were generated in-house using CRISPR (clustered regularly interspaced short palindromic repeats)-Cas9 (CRISPR-associated protein 9) technology as previously described[21].

Mice were placed on a normal chow diet (29% protein, 13% fat and 58% carbohydrate kcal; LAB Diet 5010) ad libitum with free access to water. Littermate controls were used for genetic crosses and both male and female mice were included in the study unless otherwise stated. Ages of mice used include postnatal day (P)8, P16, P21, P35, P60, P70, P90, and P120 and are indicated in the relevant experiments.

### Genotyping

Primer sequences and pairs for genotyping each of the alleles in this study are listed in Supplementary Table 1.

## Lighting conditions

Animals were housed in standard vivarium fluorescent lighting (photon flux $1.62 \times 10^{15}$ photons cm$^{-2}$s$^{-1}$) on a 12L:12D cycle except where noted. For generation of 'minus violet' animals (Extended Data Fig. 8), animals were housed in lighting chambers tuned to deliver full spectrum lighting or violet restricted lighting. For full spectrum lighting (above), light-emitting diodes (LEDs) were used to yield a comparable total photon flux of $1.642 \times 10^{15}$ photons cm$^{-2}$s$^{-1}$. Spectral and photon flux information for full spectrum LED lighting: near violet ($\lambda_{max}$=395 nm, $4.904 \times 10^{14}$ photons cm$^{-2}$s$^{-1}$ in the 375–435 nm range), blue ($\lambda_{max}$=470 nm, $4.035 \times 10^{14}$ photons cm$^{-2}$s$^{-1}$ in the 435–540 nm range), and red ($\lambda_{max}$=660 nm, $7.411 \times 10^{14}$ photons cm$^{-2}$s$^{-1}$ in the 600–700 nm range). Spectral and photon flux information for minus violet LED lighting: blue ($\lambda_{max}$=470 nm, $7.509 \times 10^{14}$ photons cm$^{-2}$s$^{-1}$ in the 435–540 nm range), and red ($\lambda_{max}$=630 nm, $9.705 \times 10^{14}$ photons cm$^{-2}$s$^{-1}$ in the 600–700 nm range), yielding a total of $1.736 \times 10^{15}$ photons cm$^{-2}$s$^{-1}$. Photon fluxes were measured at approximately 24" from source and through an empty standard mouse cage. For wavelength restricted experiments, C57BL/6J animals were housed in a 12L:12D cycle starting in late gestation (embryonic day E16.5) either in full spectrum or in minus violet. These mice are referred to in the experiments as 'full spectrum' and 'minus violet' respectively.

## Viral vectors

All viruses used in these studies were obtained from the Center for Neuroanatomy with Neurotropic Viruses (CNNV), through its partner institutions at Princeton University, University of Pittsburgh, and Thomas Jefferson University. For monosynaptic tracing of *Opn5* POA neurons, the CVS-N2c ΔG/EnvA-tdTomato rabies virus was used, derived from the deletion mutant CVS-N2c rabies strain produced in Neuro2A neuroblastoma cells. For BAT projection mapping, PRV614-mRFP1 was used, which is an attenuated laboratory pseudorabies strain expressing red fluorescent protein mRFP1 under CMV promoter control. For chemogenetic studies, AAV5-hSyn-DIO-hM3D(Gq)-mCherry and AAV5-hSyn-DIO-hM4D(Gi)-mCherry viruses were used. The CVS-N2c ΔG rabies virus was kindly provided by M.J. Schnell at Thomas Jefferson University. The PRV614-mRFP1 virus was kindly provided by L.W. Enquist at Princeton University. The AAV5-hSyn-DIO-hM3D(Gq)-mCherry and AAV5-hSyn-DIO-hM4D(Gi)-mCherry viruses were obtained through Addgene (Plasmid #44361 and #44362 respectively).

## Stereotaxic surgery

Mice were anesthetized with ventilated isoflurane (induction: 4%, maintenance: 1% - 2%), and affixed to a stereotaxic frame (Stoelting Co.). To trace preoptic *Opn5* neurons, P21 *Opn5$^{cre}$*; *R26$^{R\Phi GT/Ai6}$* mice were injected with 0.5 μL of the CVS-N2c rabies virus (titer: $1.0 \times 10^9$ PFU/mL) into the POA (coordinates relative to bregma: +0.40 mm AP, +0.20 mm ML, –4.00 mm DV). Six days post injection, mice (P27) were sacrificed and perfused with PBS and 4% paraformaldehyde. For BAT projection mapping, P60 *Opn5$^{cre}$*; *R26$^{Ai6/Ai6}$* mice were dissected to expose the interscapular adipose region. Six 50 nL nanoinjections of the PRV614-mRFP1 virus (titer: $4.9 \times 10^9$ PFU/mL) were made bilaterally into the interscapular brown adipose tissue. Mice were then sacrificed and perfused with PBS and 4%

paraformaldehyde five days post-injection. For chemogenetic studies, 4 week old male *Opn5^cre/+^*, *Opn5^cre/-^* (*Opn5* reporter null), and *Opn5^+/+^* (cre-negative control) mice were injected with 1.0 µL AAV5-hSyn-DIO-hM3D(Gq)-mCherry or AAV5-hSyn-DIO-hM4D(Gi)-mCherry virus (titer: $7 \times 10^{12}$ vg/mL) into the POA (coordinates relative to bregma: +0.40 mm AP, +0.20 mm ML, −4.00 mm DV). All AAV-injected mice were given a recovery period of at least 2 weeks prior to further experimentation.

**Chemogenetic manipulation experiments**

Implanted mice were transferred to the lighting chamber that was situated in either cold (4°C) or room temperature (22°C) conditions for chemogenetic inhibitory hM4D(Gi) experiments, or just room temperature (22°C) for chemogenetic stimulatory hM3D(Gq) experiments. BAT and core temperature recordings were collected every 5 minutes for a total of 5 hours, from 10AM – 3PM. Lighting conditions were maintained with red (660 nm), blue (480 nm) and violet (380 nm) for the entire 5 hours. At hour 2, either CNO (1.0 mg/kg Gq DREADD, 2.0 mg/kg for Gi DREADD or vehicle (saline) was administered intraperitoneally to animals. All animals received both CNO and vehicle in separate experiments, and once telemetric recordings were complete, animals were administered CNO and sacrificed 6 hours later, with relevant tissues harvested and the telemetric sensor explanted.

**Thermoregulation and cold exposure assays**

Core body temperature assessment upon acute cold exposure was performed as previously described[7] on *Opn5* null (*Opn5^−/−^*) and littermate controls (*Opn5^+/+^*). Mice with *Opn5* conditionally deleted from the retinal progenitors (*Opn5^fl/fl^* and *Rx-cre; Opn5^fl/fl^*), and *Opn5* conditionally deleted from *Lepr*-expressing neurons in the POA (*Opn5^fl/fl^* and *Lepr-cre; Opn5^fl/fl^*) were also subjected to this assay. Furthermore, enucleated *Opn5^+/+^* and *Opn5^−/−^* mice, and 'full spectrum' and 'minus violet' reared C57BL/6J animals were also cold exposed.

P60 adult male and female littermates were separated from their home cage and individually housed in a home-built lighting chamber situated in an electronically monitored 4°C cold room for 3 or 5 hours depending on the assay. While the mouse was conscious, core body temperature was measured with a RET-3 microprobe rectal thermometer (Kent Scientific Corporation, Torrington, CT) every 20 minutes for the duration of the assay. Food and water were available *ad libitum*. The thermometer probe operator was blinded to mouse genotype and prior temperature measurements throughout the experiment. At the end of the cold exposure, mice were euthanized and relevant tissues (BAT, inWAT, pgWAT) were dissected, weighed, and snap frozen for downstream molecular profiling.

For all 3 hour cold exposure assays, animals were subjected to a red (660 nm), blue (480 nm), and violet (380 nm) LED combination (RBV). For 5 hour cold exposure assays, animals were initially subjected to only red (660 nm) and blue (480 nm) lighting (RB) for the first three hours. After the initial 3 hours, violet light (380 nm) was then supplemented during hours 4 and 5. All 3 hour cold exposure assays were performed during the animals'

subjective day from 11AM – 2PM. The 5 hour assays were all performed from 10AM – 3PM.

### Telemetric temperature monitoring

P60 adult male *Opn5* null mice (*Opn5$^{-/-}$*) and wild type littermate controls (*Opn5$^{+/+}$*), and *Opn5$^{cre}$; AAV5-hM3D(Gq)* or *AAV5-hM4D(Gi)* injected mice were implanted with indwelling telemetric sensors and subjected to a 5 hour cold (4°C) or ambient (22°C) temperature exposure assay. *Opn5$^{cre}$; AAV5-hM3D(Gq)* animals did not undergo a cold exposure assay. In brief, animals were moved to individual housing and acclimated to a soft diet (DietGel® 76A, and DietGel® Recovery + 1mg/2oz carprofen) 3 days prior to the implantation surgery. On the day of the surgery, animals were anesthetized and maintained with ventilated isoflurane, and a telemetric sensor (TTA-XS, Stellar Telemetry, TSE Systems) was subcutaneously implanted in the dorsal cavity. The sensor wirelessly communicates with an external antenna, and features two external thermistor leads, one advanced underneath the iAT (BAT temperature), and one advanced through the peritoneum to rest in the visceral cavity of the mouse (core temperature). Telemetric data was acquired using BIOPAC AcqKnowledge 5.0 software. Implanted mice were returned to individual housing and monitored for at least two weeks prior to experiments.

### Acute violet light stimulation experiments

Implanted mice were transferred to a home-built lighting chamber that was situated either in the cold (4°C) or in room temperature (22°C). BAT and core temperature readings were collected every 5 minutes for a total of 5 hours, from 10AM – 3PM. Lighting conditions were either maintained with red (660 nm) and blue (480 nm) for the entire 5 hours, or with violet (380 nm) light supplemented for hours 4 and 5. Following the experiment, mice were either returned to light-controlled housing, or sacrificed and perfused with 4% paraformaldehyde, with relevant tissues harvested and the telemetric sensor explanted.

### Imaging intracellular cAMP dynamics

Two-photon imaging of intracellular cAMP dynamics *ex vivo* in acute brain slices was performed as follows.

### Acute brain slice preparation

P30-P60 *Opn5$^{cre/+}$; CAMPER* or *Opn5$^{cre/-}$; CAMPER* male and female mice were dark adapted for four hours prior to tissue harvest. Ice-cold modified artificial cerebrospinal fluid (mACSF, 92 mM NaCl, 2.5 mM KCl, 1.25 mM NaH$_2$PO$_4$, 30 mM NaHCO$_3$, 25 mM glucose, 20 mM HEPES, 5 mM Na-ascorbate, 3 mM Na-pyruvate, 2 mM thiourea, 10 mM MgSO$_4$·7H$_2$O, 0.5 mM CaCl$_2$·2H$_2$O, titrated to pH=7.22 by NaOH) was equilibrated with 95% oxygen and 5% carbon dioxide. Under dim red light, mice were anesthetized with isoflurane, thoracotamized, and transcardially perfused with oxygenated ice-cold mACSF. Brains were rapidly dissected and placed in oxygenated ice-cold mACSF. Coronal 300 μm sections were cut with a vibratome (Leica® VT1000 S) and placed in a foil-covered bubbled room-temperature *N*-methyl-D-glucamine recovery solution (NMDG, 92 mM *N*-methyl-D-glucamine, 2.5 mM KCl, 1.25 mM NaH$_2$PO$_4$, 30 mM NaHCO$_3$, 25 mM glucose, 20 mM

HEPES, 5 mM Na-ascorbate, 3 mM Na-pyruvate, 2 mM thiourea, 10 mM $MgSO_4 \cdot 7H_2O$, 0.5 mM $CaCl_2 \cdot 2H_2O$, 92 mM *N*-methyl-D-glucamine, titrated to pH=7.25 by HCl) for 30 minutes. To record intracellular cAMP dynamics, slices were transferred to a recording chamber (RC-26G, Werner Instruments) and continuously perfused with 30–34°C oxygenated mACSF at a rate of 2.1 mL/min. To isolate responses intrinsic to hypothalamic neurons, the perfused mACSF was supplemented with 1 μM tetrodotoxin citrate (HB1035, Hello Bio) during imaging.

### Brain slice imaging

Two-photon imaging of FRET was performed on a Nikon A1R upright confocal microscope using the NIS Elements Confocal software package v5.20.02. Images were acquired through a 16x dipping objective (CFI75 LWD 16X W, Nikon). mTurquoise (FRET donor) was excited by tuning a TiSapphire IR laser to 850 nm for two-photon imaging, with 470 – 500 nm (mTurquoise; FRET donor, CFP channel) and 525 – 575 nm (cp173Venus-Venus; FRET acceptor, YFP channel) bandpass emission filtration. To visually locate *Rapgef3*-expressing cells, the POA was briefly exposed to blue epifluorescence of 488 nm for less than a minute. For dark-treated and drug-treated cells, images were taken every minute. For 405 nm-laser illuminated cells, images were taken every other minute, with one minute of continuous 405 nm photostimulation in between. Drugs were bath-applied at the 45 minute mark of the experiment. 20 μM forskolin NKH477 (344281, EMD Millipore), 200 μM IBMX (02195262-CF, MP Biomedicals), and 10 μg/mL digitonin (D141, Sigma Aldrich) were applied according to experimental timepoints. F (change in FRET) is presented as the ratio of donor emission to acceptor emission (CFP/YFP). Images were processed and quantified using NIS Elements AR v5.20.00, ImageJ Ratio Plus plugin, and MATLAB 2018a.

### Indirect calorimetry

Male and female *Opn5*$^{+/+}$ and *Opn5*$^{-/-}$ mice aged P90-P120 were acclimated in metabolic chambers (PhenoMaster®, TSE Systems GmbH, Germany) for 3 days before the start of the study. Mice were continuously recorded for a total of 16 days with the following measurements taken every 15 minutes: gas exchange ($O_2$ and $CO_2$), food intake, water intake, and spontaneous locomotor activity (in the XY plane). Ambient temperature was adjusted via climate-controlled chambers that housed the metabolic chambers. $VO_2$, $VCO_2$, and energy expenditure (EE) were calculated according to the manufacturer's guidelines (PhenoMaster® Software, TSE Systems GmbH, Germany), with EE estimated via the abbreviated Weir formula. The respiratory exchange ratio (RER) was calculated by the ratio $VCO_2/VO_2$. Mass-dependent variables ($VO_2$, $VCO_2$, EE) were not normalized to body weight. Food and water intake were measured by top-fixed load cell sensors, from which food and water containers were suspended into the sealed cage environment. For food consumption, mice demonstrating excessive food grinding behavior were excluded from statistical analyses. After 8 days of continuous recording, cages were replaced with clean ones and sealed, and gas exchange re-equilibration completed all within 4 hours. Body mass composition (fat and lean mass) were measured using nuclear magnetic resonance and expressed as grams of fat and lean tissue, and as a percentage of total body mass.

For CL-316,243 experiments, mice aged P90-P120 were acclimated in metabolic chambers (Promethion, Sable Systems International) for 3 days prior to the start of the study. Male and female $Opn5^{+/+}$, $Opn5^{-/-}$, full spectrum, and minus violet mice were included for these studies. Oxygen consumption ($VO_2$), carbon dioxide production ($CO_2$), energy expenditure (EE), respiratory exchange ratio (RER), and locomotor activity (cm/s) were recorded every 5 minutes using Sable Systems International Metascreen software v2.3.15.11. Food and water were available *ad libitum*. 1.0 mg/kg CL316,243 or vehicle (saline) was intraperitoneally injected at hour 1 of a six-hour measurement window between 11AM – 5PM. All animals received both CL316,243 and vehicle injections in randomized order. Data was exported using Sable Systems International ExpeData software v1.9.27.

### Infrared thermography (FLIR)

For whole-body infrared thermographic imaging, adult (P90) and neonatal (P8) $Opn5^{+/+}$ and $Opn5^{-/-}$ mice were individually housed and placed in a home-built lighting chamber situated in 4°C for 30 minutes. IR thermographic images were taken with a FLIR T530 infrared camera (FLIR® Systems, Wilsonville, OR) every minute for a total of 30 images per P90 adult or pair of P8 pups. To quantify interscapular region temperature, a pixel average from a region of interest drawn over the iAT was taken per image per mouse using FLIR Tools Desktop software v5.13.18031.2002. The size of the selected region of interest did not change. For the comparative IR images, P90 adult mice were briefly anesthetized after the 30 minute cold exposure and laid side by side. To quantify surface tail temperature of adult $Opn5^{+/+}$ and $Opn5^{-/-}$ mice, animals were placed in a tubular mouse restraint (Kent Scientific Corporation, Torrington, CT). These restraints permitted respiration through a slotted nose cone but immobilized the animal while exposing its tail through a rear port. Tail temperatures were quantified by describing a pixel-averaged circular region of interest of consistent size and rostrocaudal distance from the base of the tail, per minute, per mouse.

### video tracking

P60 male $Opn5^{+/+}$ and $Opn5^{-/-}$ mice were placed in custom built cylindrical open-top acrylic enclosures with paper bedding and enrichment situated in an electronically monitored 4°C cold room. A recording camera (Fujifilm XT-10, with Samyang 12mm f/2.0 lens) was affixed approximately 24" above the cages and recorded video at 24 frames per second for a total of 140 minutes. Ambient 480 nm and 660 nm LEDs provided red and blue illumination, and at the 80 minute mark, 380 nm violet LEDs were switched on. The video was re-encoded at 2.4 frames per second and analyzed by centroid-based motion tracking in NIS Elements Ar v5.20.00.

### Noninvasive blood pressure measurements

Animals were acclimated to a tubular mouse restraint (Kent Scientific Corporation) situated on a heated stage for 2–3 days prior to the study. On the day of the experiment, animals were placed inside the restraint on a heated stage and connected to a tail occlusion cuff and a volume pressure recording (VPR) cuff that communicated with the CODA™ High Throughput Noninvasive Blood Pressure System (Kent Scientific Corporation). 30 trials of tail occlusion and VPR recordings were automatically and sequentially gathered per animal,

and systolic/diastolic blood pressure, mean arterial pressure, and pulse rate calculated by the CODA™ Data Acquisition Software v4.1.

### Intra-Adipose Tissue Radiometry

Fabrication of the Holt-Sweeney microprobe was performed as previously described[30]. The termination of one end of a 100 μm silica core fiber optic patch cable (Ocean Optics, Dunedin, FL, USA) was removed. The fiber's furcation tubing and jacketing was stripped, and the fiber's polyimide buffer was removed 5 cm from the fiber's end using a butane torch. A 10 g weight was attached to the end of the fiber and then pulled upon heating with the butane torch, narrowing the diameter. The narrowed region of the fiber was then cut using carborundum paper, to yield a flat fiber end with a diameter of 30 – 50 μm. The sides of the narrowed fiber were painted with a film opaquing pen to prevent stray light from entering, while leaving a small transparent opening at the fiber tip. For structural support, this bare, tapered fiber was then secured in the tip of a pulled glass Pasteur pipette using a drop of cyanoacrylate glue, leaving only 6–9 mm of bare optical fiber protruding. A small light-scattering ball was added to the end of the tapered optical fiber for spectral scalar irradiance measurements. To do this, titanium dioxide was thoroughly mixed with a high-viscosity UV-curable resin, DELO-PHOTOBOND, GB368 (DELO Industrie Klebstoffe, Windach, Germany). The tip of a pulled fiber was quickly inserted and removed from a droplet of the resin and titanium dioxide mixture, resulting in a sphere with a diameter of approximately twice that of the tapered fiber. As all measurements from a given probe were normalized to the signal from the same probe in a gelatin blank, small variations in the probe diameter have no effect on our results. The sphere was cured for 12 h using a Thorlabs fiber coupled LED light source (M375F2, Thorlabs Inc, Newton, NJ, USA).

For intra-tissue radiometric measurements in mice, animals were anesthetized under ventilated isoflurane and placed in a mouse stereotaxic frame (Stoelting Co, Wood Dale, IL, USA). Hair over the scalp was shaved and the skin incised rostrocaudally to expose the skull surface. The skull was breached with a small 0.5 mm diameter micromotor drill 0.4 mm anterior and 0.2 mm lateral to bregma. Following, the Holt-Sweeney microprobe was affixed to the stereotaxic frame, positioned over AP +0.40 mm, ML +0.20 mm, and lowered to DL −4.00 mm in 0.50 mm increments. While the probe is in position, the scalp skin was repositioned to cover as much of the incision site as possible without obstructing probe descent. For broadband light illumination, a Thorlabs plasma light source (HPLS345, Thorlabs Inc, Newton, NJ, USA) was positioned above and in front of the mouse stereotaxic frame. The light was delivered to the animal via a 5 mm liquid light guide connected to a 2 in. collimating lens secured in a vice. The distance from the collimating lens to the animal was approximately 2 ft.

Scalar irradiance measurements as a function of wavelength were obtained at the surface of the cortex and at probe depth increments of 0.50 mm up to 4.00 mm. Spectral irradiance data was collected using an Ocean Optics 200–850 nm spectrometer (JAZ Series, Ocean Optics, Dunedin. FL, USA) and recorded using Ocean Optics OceanView v1.6.5 software.

### Tissue processing, sectioning, and immunohistochemistry

Animals were anesthetized under isoflurane and transcardially perfused with 4% paraformaldehyde solution. For immunofluorescence, brains were dissected and post-fixed in cold 4% paraformaldehyde overnight at 4°C. After washing in PBS, brains were cryoprotected in sucrose solution and embedded for sectioning in a cryostat (Leica® CM3050 S). 30 μm sections were obtained and subsequently processed for immunofluorescence (IF). For immunohistochemistry, iAT and inWAT tissues were dissected and post-fixed in 4% paraformaldehyde overnight at room temperature. After washing in PBS, tissues were processed (Leica® ASP300S) and embedded (Tissue-Tek® TEC™ 6). Embedded tissue blocks were cut using a microtome (Leica® RM2255) at a thickness of 4.5 μm. Slides were incubated overnight at 4°C in primary, rinsed, and then incubated in secondary for 1 hour at room temperature. Slides were then rinsed and mounted with VectaShield® HardSet™ antifade mounting medium with DAPI.

Antibodies used for IF include NeuroTrace™ 435/455 blue fluorescent Nissl stain (ThermoFisher Scientific, N21479, 1:100 dilution), anti-Isolectin IB4 antibody (ThermoFisher Scientific, I21411, 1:300 dilution), anti-Tyrosine Hydroxylase antibody (Abcam, ab113, 1:500 dilution), and anti-insulin antibody (Dako, A0564, 1:500 dilution). Antibodies used for IHC include anti-UCP1 antibody (Abcam, ab10983, 1:500 dilution).

### Xgal staining

For Xgal labelling, P10 *Opn5^lacZ* and P16 *Lepr-cre; Ai14; Opn5^lacZ* animals were anesthetized and transcardially perfused with Xgal fixative (1% formaldehyde, 0.2% glutaraldehyde, 2 mM $MgCl_2$, 5 mM EGTA, and 0.01% Nonidet P-40). Brains were dissected and post-fixed in cold Xgal fixative overnight at 4°C. Brains were then washed and cryoprotected as described above and then labeled with Xgal enzyme. The reaction was monitored closely and stopped when background started to appear in control (lacZ negative) tissues. Following four washes in PBS, 30 μm cryosections from *Opn5^lacZ* animals were briefly post-fixed in 4% paraformaldehyde, counterstained with Nuclear Fast Red, dehydrated, and then imaged under standard transmitted brightfield using Zeiss AxioVision v4.9.1 SP2 software. For *Lepr-cre; Ai14; Opn5^lacZ* cryosections, the Nuclear Fast Red counterstain was not applied.

### Cell size quantification (inWAT)

Hematoxylin stained paraffin sectioned inWAT samples were imaged under 594 nm excitation through a rhodamine filter. Monochrome images were thresholded and adipocyte cell boundaries automatically detected using NIS Elements Advanced Research v5.20.00 software (Nikon Instruments Inc.). Individual cells were demarcated as separate objects in a binary layer, filtered for circularity and size, and their area measured in $\mu m^2$. Approximately 500 – 1000 cells were measured per field, with at least 20 fields per animal analyzed, for a total of 10,000 – 20,000 cells per animal. Cell areas were binned into 100 $\mu m^2$ intervals and the frequency of total cells (%) charted for each interval.

### Multiplex fluorescence *in situ* hybridization (M-FISH)

M-FISH experiments were performed with fresh-frozen brain tissue. Briefly, P21 male and female *Opn5*<sup>cre/+</sup>; *Ai14* mice were sacrificed and their brains rapidly dissected into cryo-embedding medium. Embedded brains were snap-frozen in liquid nitrogen, and 14 µm cryosections of the POA were obtained and processed for M-FISH using the RNAscope® Fluorescent Multiplex Reagent Kit V1 (ACDBio). Probes against the following mRNAs were used: *Slc32a1* (Vgat), *Slc17a6* (Vglut2), *Adcyap1* (PACAP), *Bdnf* (BDNF), and *tdTomato*. *In situ* hybridization was performed as per the manufacturer's protocol for fresh frozen tissue. Briefly, POA sections were pretreated by serial immersion of the slides in 1x PBS, nuclease-free water, and 100% EtOH at room temperature for two minutes each. Probe hybridization was achieved by incubating sections in 40 µL of mRNA target probes for 2 hours at 40°C, followed by signal amplification using manufacturer-provided Amp1, Amp2, Amp3, and Amp4 reagents for 30, 15, 30, and 15 minutes respectively at 40°C. Each incubation step was followed by two 2-min washes of manufacturer-provided wash buffer. Slides were mounted using Tris-buffered Fluoro-Gel mounting medium (Electron Microscopy Sciences).

### M-FISH quantification

60x fields were acquired from *Opn5*<sup>cre/+</sup>; *Ai14* POA regions from $n=3$ animals. Prior to cell counting, negative control regions of interest (ROI) were acquired. Single cell images ($715\mu m^2$ ROIs) of ependymal cells or dural cells were acquired to calculate background labeling for all 3 channels, which varied across experiments and probes. Using the nuclear marker channel (DAPI) and *tdTomato* (C2) probe, several $715\mu m^2$ ROIs were acquired representing cells of interest. Then, puncta from C1 (*Slc32a1* or *Bdnf*) and C3 (*Slc17a6* or *Adcyap1*) for each ROI was calculated and the cell was assessed to be positive or negative for a marker. Cells were considered positive if the number of puncta was 1.5x above background for that section. Total of 109 cells from $n=3$ animals were used for *Slc32a1* and *Slc17a6* assessment, and a total of 97 cells from $n=3$ animals were used for *Bdnf* and *Adcyap1* assessment.

### Serum lipids and thyroid hormones

Serum from P90-P120 *Opn5*<sup>+/+</sup> and *Opn5*<sup>−/−</sup> male and female mice were harvested and snap frozen. Lipid profiles (TG, PL, CHOL, NEFA) were obtained via standard colorimetric methods performed at the University of Cincinnati Mouse Metabolic Phenotyping Center (NIH 2U2C-DK059630–16). Briefly, triglyceride quantification was performed by the GPO-PAP method (Randox), phospholipids by the choline oxidase-DAOS method (Wako Diagnostics), cholesterol by the Infinity™ cholesterol liquid stable reagent method (Thermo Scientific), and NEFAs by the ACS-ACOD method (Wako Diagnostics). Colorimetric measurements were obtained using a Synergy HT (BioTek) with Gen5 software. Serum measurements of free thyroxine (T4) and thyrotropin releasing hormone (TRH) were made using competitive ELISA and performed at the University of Massachusetts MMPC (NIH 5U2C-DK093000–07).

### Western blotting

Western blots were performed using standard protocols. BAT from animals were dissected into 400 μL of modified RIPA lysis buffer and homogenized (Tissue Lyser II, Qiagen) using zirconium oxide beads (2.0 mm). After centrifugation and protein quantification (Pierce™ BCA Protein Assay Kit), 10 μg protein were loaded onto a 16% Novex Tris-Glycine protein gel and transferred to a PVDF (polyvinylidene difluoride) membrane, where bands were visualized by chemiluminescence. Antibodies used for western blotting include anti-UCP1 (Abcam, ab10983, 1:5000 dilution) and anti-alpha tubulin (Abcam, ab4074, 1:5000 dilution).

### Quantitative RT-PCR

Intrascapular adipose depots were harvested immediately following cold exposure assays. Snap frozen tissue was homogenized in TRI Reagent (Invitrogen) using RNase-free zirconium oxide beads (2.0 mm) in a TissueLyser II sample disrupter (Qiagen). Phase separation was accomplished via chloroform and RNA in the aqueous phase was precipitated with ethanol and column-purified via the GeneJET RNA purification kit (ThermoFisher Scientific #K0732). Purified RNA was subsequently treated with RNase-free DNase I (ThermoFisher Scientific #EN0521) and cDNA was synthesized using a Verso cDNA synthesis kit (ThermoFisher Scientific AB1453/B). Quantitative RT-PCR was performed with Radiant™ SYBR Green Lo-ROX qPCR mix (Alkali Scientific Inc.) in a ThermoFisher QuantStudio 6 & 7 Flex Real-Time PCR system. Primer information for quantitative PCR is included in Supplementary Table 2. Relative expression was calculated by the CT method using *Tbp* (TATA binding protein) as the normalizing gene. Statistical significance was calculated by a two-way ANOVA followed by Tukey post-hoc analysis, using a p-value cutoff of 0.05.

### Statistics and reproducibility

Statistical and image analyses were performed with MATLAB 2018a, NIS Elements Ar v.5.20.00, and ImageJ. Sample sizes for each experiment are reported in the manuscript or in the figures. The numbers of experimental repitions were as follows: Fig. 1a, b, 12 times; Fig. 1c, d, 3 times; Fig. 1e–k, 3 times; Fig. 1l–x, 7 times; Fig. 2a–i, 5 times; Fig. 2j–u, 4 times; Fig. 3a–d, 5 times; Fig. 3e, twice; Fig. 3f–h, twice; Fig. 4a–k, 4 times; Extended Data Fig. 1a–k, 3 times; Extended Data Fig. 2a–c, 3 times; Extended Data Fig. 3a–l, 4 times; Extended Data Fig. 4a, 3 times, Extended Data Fig. 4b, twice (22°C), once (4°C). Extended Data Fig. 4c–e, 3 times; Extended Data Fig. 4f, g, 3 times; Extended Data Fig. 4h, i, once; Extended Data Fig. 4j–m, 4 times; Extended Data Fig. 4n–q, 3 times; Extended Data Fig. 4r, three times; Extended Data Fig. 4s, twice (22°C), once (4°C). Extended Data Fig. 4t–v, 3 times; Extended Data Fig. 5a–g, twice; Extended Data Fig. 6a–f, twice; Extended Data Fig. 6g–i, 3 times; Extended Data Fig. 6j–l, twice; Extended Data Fig. 6m, 3 times; Extended Data Fig. 7a–g, 3 times; Extended Data Fig. 8a–i, 6 times; Extended Data Fig. 9c, 3 times; Extended Data Fig. 9d, twice; Extended Data Fig. 9e–g, 3 times; Extended Data Fig. 9h, i, twice; Extended Data Fig. 9j–m, 3 times; Extended Data Fig. 10a–e, 3 times.

## Reporting Summary

Further information on research design is available in the Nature Research Reporting Summary linked to this article.

## Data availability

Source data in Excel and MATLAB format for all experiments in this study are available under "Source Data" in this article. All other relevant data are available from the corresponding authors upon request.

## Extended Data
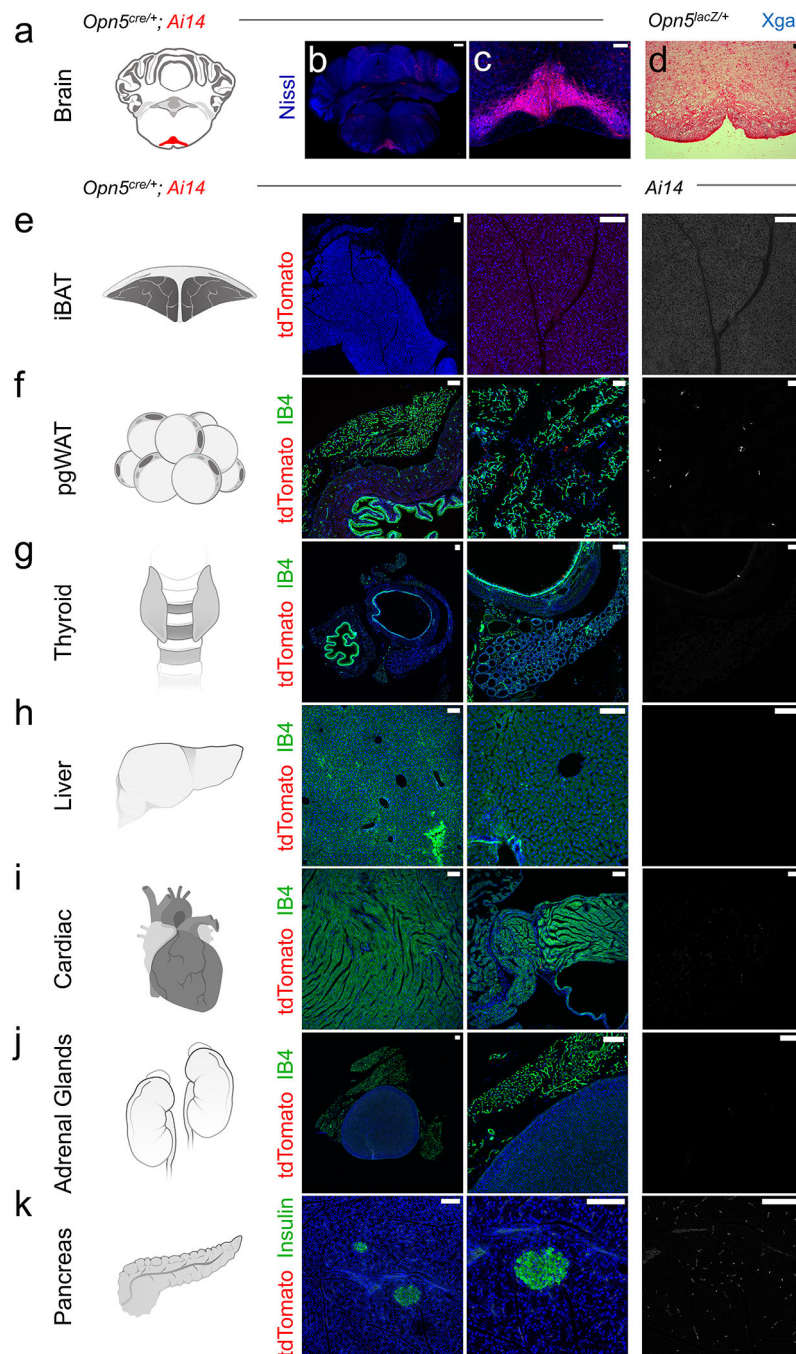


**Extended Data Fig. 1 |.** ***Opn5*** **lineage survey across the CNS and thermogenic organs.**
**a-c,** Brain atlas representation (**a**) and coronal brain sections (**b, c**) of P21 *Opn5cre/+; Ai14*
mouse highlighting tdTomato expression (red) in the raphe pallidus (RPa). **d,** Coronal brain
section from P10 *Opn5lacZ/+* mouse showing that the RPa is negative for Xgal labeling. **e-k,**
Representative confocal images from IB4 labeled (green) P35 *Opn5cre/+; Ai14* (expressing
tdTomato, red) tissues across the organism. (**e**) Interscapular brown adipose tissue (iBAT),

(**f**) perigonadal white adipose tissue (pgWAT), (**g**) thyroid gland, (**h**) liver, (**i**) cardiac muscle, (**j**) adrenal glands, and (**k**) pancreas. Scale bars, 100 μm (**e-k**), 150 μm (**c, d**), 500 μm (**b**).
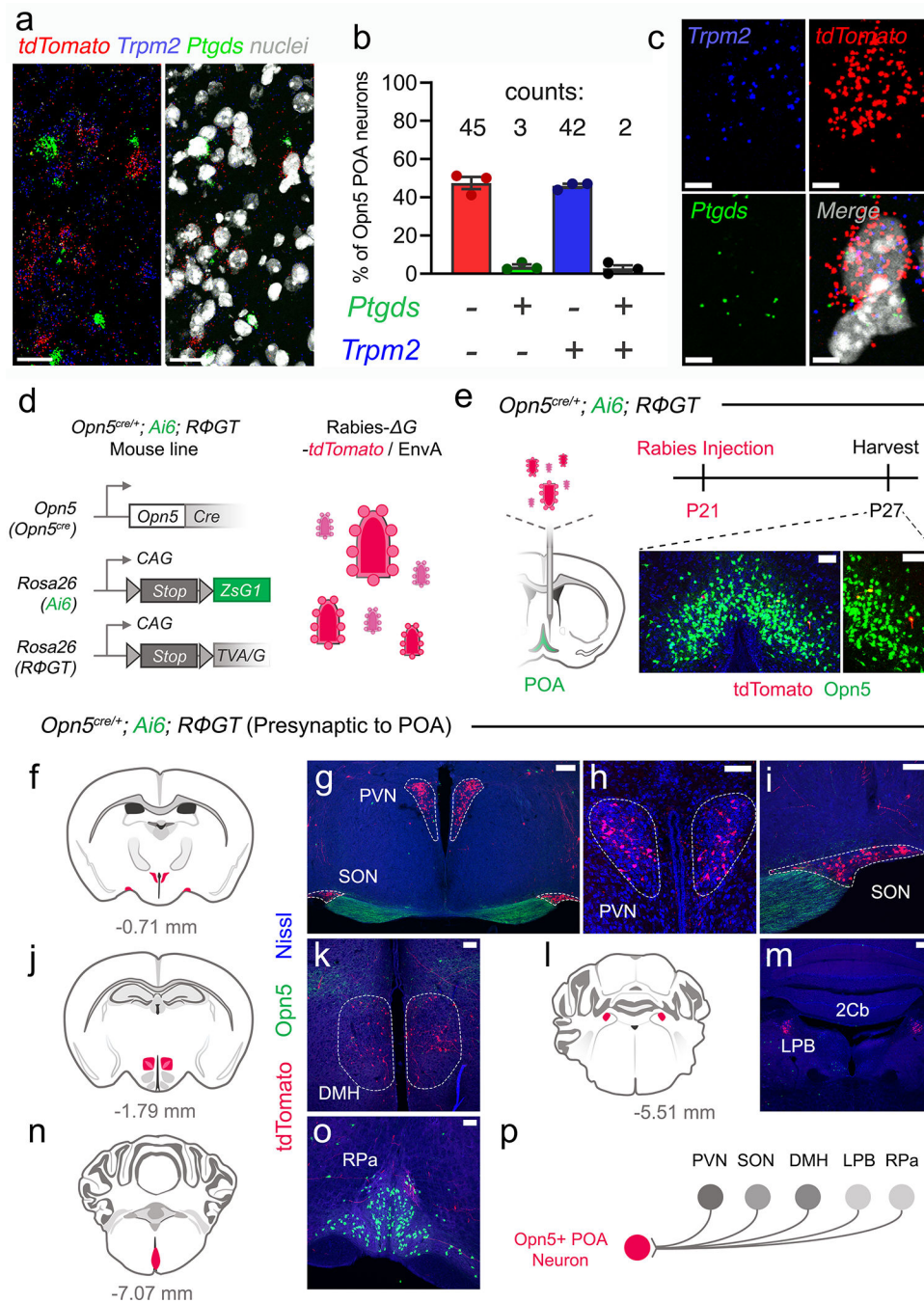


**Extended Data Fig. 2 |. M-FISH of *Opn5* POA neurons against *Ptgds* and *Trpm2*.**
**a,** Representative images of *Opn5*<sup>cre/+</sup>*; Ai14* POA neurons probed for *Ptgds* (green), *tdTomato* (red), *Trpm2* (blue) and labeled with DAPI for nuclei (greyscale) with corresponding quantification (**b**) of overlap (*n*=3 animals; 92 cells). **c,** Representative images of *Opn5*<sup>cre/+</sup>*; Ai14* cells (red) also positive for *Trpm2* (blue) but *Ptgds* labeling (green) that

is below the background labeling threshold. Scale bars, 5 μm (**c**), 25 μm (**a**). Data in **b** are mean ± s.e.m.
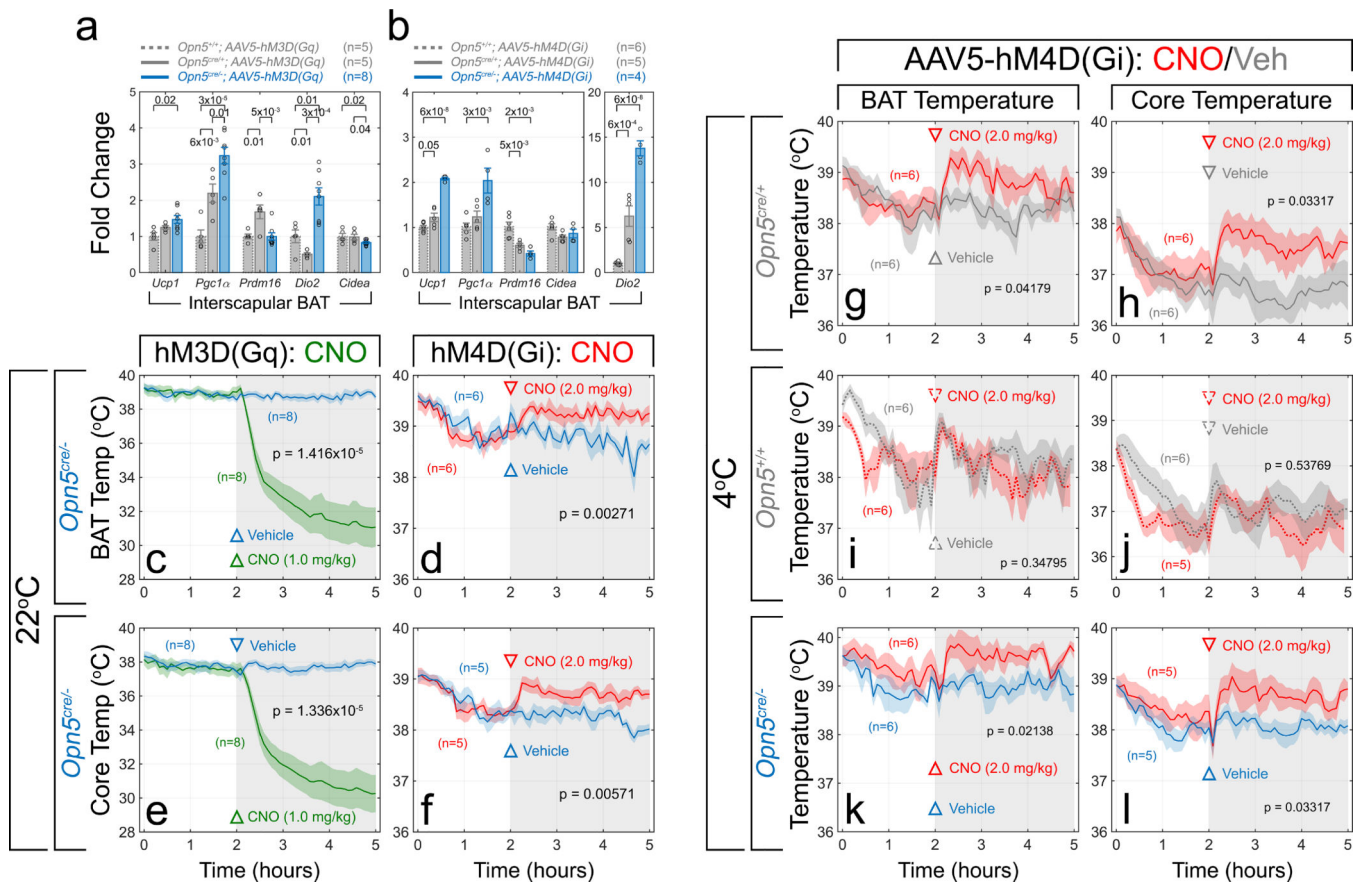


**Extended Data Fig. 3 |. Thermoregulation by *Opn5* POA neurons is not context-dependent.**
**a, b,** QPCR of thermogenesis genes in iBAT 6h post-CNO induction in mice with viral-mediated expression of stimulatory hM3D(Gq) DREADD (**a**) or inhibitory hM4D(Gi) DREADD (**b**) in the POA. (**a**) *Opn5$^{+/+}$* (*n*=5), *Opn5$^{cre/+}$* (*n*=5), and *Opn5$^{cre/-}$* (*n*=8). (**b**) *Opn5$^{+/+}$* (*n*=6), *Opn5$^{cre/+}$* (*n*=5), and *Opn5$^{cre/-}$* (*n*=4). p values are indicated above the bars. **c-f,** Similar to Figure 2, *Opn5$^{cre/-}$* POA were injected with AAV5-hM3D(Gq) DREADD (**c**, **e**; *n*=8 animals per condition) or AAV5-hM4D(Gi) DREADD (**d**, **f**; *n*=6 animals per condition). Telemetric BAT and core recordings following intraperitoneal administration of CNO or vehicle (open arrowheads) at the 2 hour mark. **g-l,** *Opn5$^{+/+}$*, *Opn5$^{cre/+}$*, *Opn5$^{cre/-}$* (*n*=6 per genotype and condition) mice were injected with AAV5-hM4D(Gi) DREADD, and followed by chemogenetic manipulations as previously described, but at 4°C ambient temperature. All data are mean ± s.e.m. *p* values are from (**a**, **b**) ANOVA with Tukey post-hoc analysis, (**c-l**) 1-way repeated measures ANOVA.
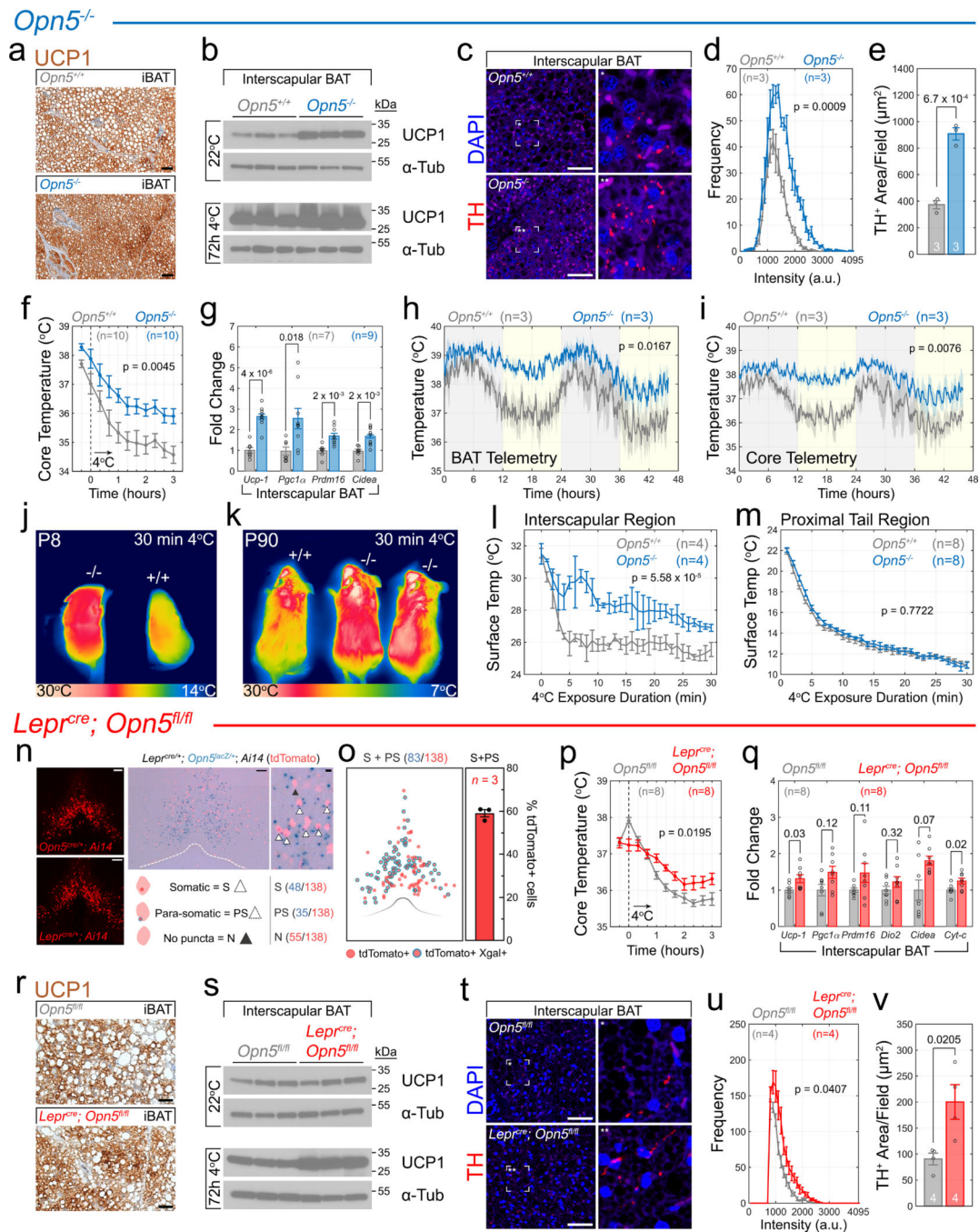
**Extended Data Fig. 4 |. *Opn5* loss-of-function exaggerates BAT thermogenesis.**
**a,** Immunohistochemistry for UCP1 protein in iBAT from *Opn5+/+* and *Opn5−/−* mice. **b,**
UCP1 immunoblots for iBAT comparing ambient temperature (22°C) and 72 hour 4°C
exposure for *Opn5+/+* (*n*=3) and *Opn5−/−* (*n*=3) mice. **c-e,** Representative IF of TH+
(tyrosine hydroxylase) innervation of iBAT (**c**) used for quantification in (**d**, **e**). **f,** Core
temperature assessment (rectal) of *Opn5+/+* and *Opn5−/−* mice during 3h cold exposure. **g,**
QPCR of thermogenesis genes (*Ucp1, Pgc1a, Prdm16, Cidea*) in iBAT from mice in (**f**). **h, i,**
48h assessment of body temperature rhythms in *Opn5+/+* (n=3 animals) and *Opn5−/−* (n=3

animals) mice using telemetry sensors in iBAT (**h**) and core (**i**) under 12L:12D lighting conditions. **j, k,** Infrared thermography of P8 (**j**) and P90 (**k**) *Opn5$^{+/+}$* and *Opn5$^{-/-}$* mice following 30 min cold challenge. **l, m,** Quantification of thermographic images focused on interscapular region (**l**), and tail (**m**). **n,** Representative POA images from *Opn5$^{cre/+}$; Ai14* and *Lepr$^{cre/+}$; Ai14* animals, plus *Lepr$^{cre/+}$; Ai14* colocalization with *Opn5$^{lacZ/+}$* expression (Xgal). **o,** Quantification of overlap in (**n**). **p,** Core temperature assessment (rectal) of control (*Opn5$^{fl/fl}$*) and *Lepr$^{cre}$; Opn5$^{fl/fl}$* mice during 3h cold challenge. **q,** QPCR of thermogenesis genes in iBAT from mice in (**p**). **r,** Immunohistochemistry for UCP1 protein in iBAT from *Opn5$^{fl/fl}$* and *Lepr$^{cre}$; Opn5$^{fl/fl}$* mice. **s,** UCP1 immunoblots for iBAT comparing ambient temperature (22°C) and 72 hour 4°C exposure for *Opn5$^{fl/fl}$* ($n$=3) and *Lepr$^{cre}$; Opn5$^{fl/fl}$* ($n$=3) mice. **t-v,** Representative IF of TH+ innervation of iBAT (**t**) used for quantification in (**u, v**). Scale bars, 50 μm (**a, c, r, t**), 100 μm (**n**). Data are mean ± s.e.m. *p* values are from (**d, f, h, i, l, m, p, u**) 1-way repeated measures ANOVA, (**g, q**) ANOVA with Tukey post-hoc analysis, (**e, v**) two-tailed Student's *t*-test.
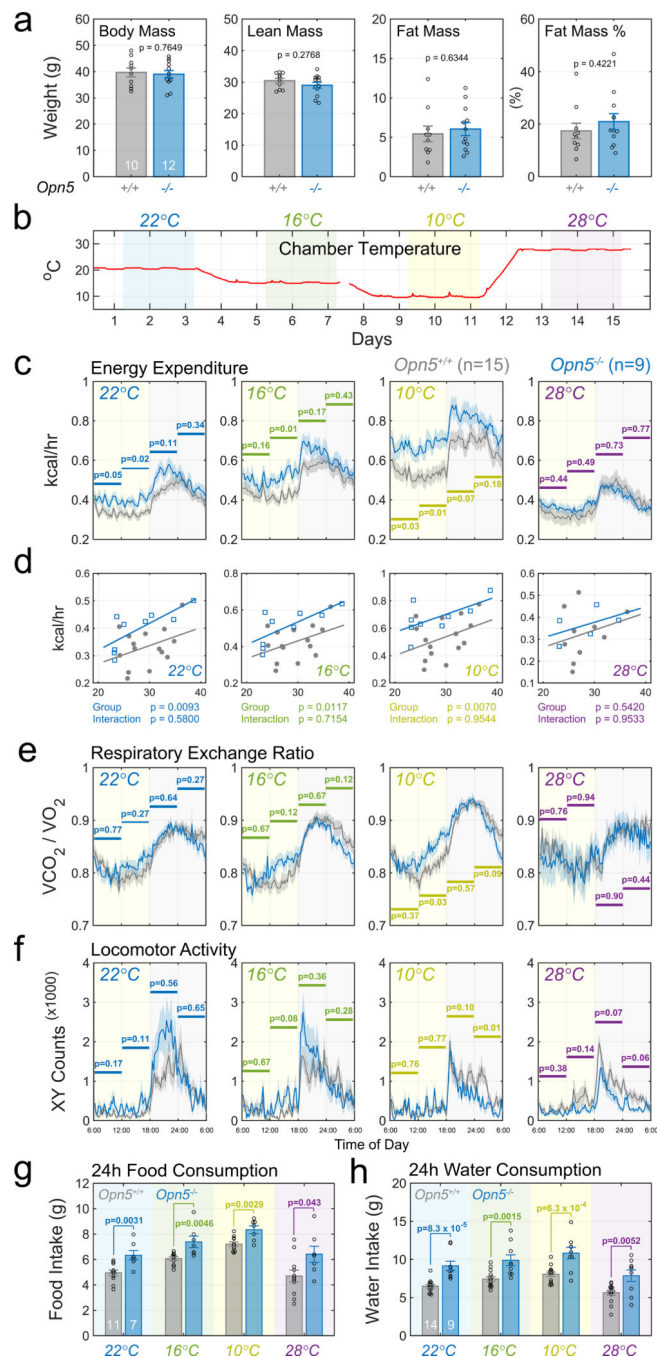
**Extended Data Fig. 5 |. *Opn5* null mice have altered energy homeostasis.**
**a,** Body mass, body composition (lean mass/fat mass), and fat mass as a percentage of body
mass (fat mass %) comparison between *Opn5^{+/+}* (*n*=10) and *Opn5^{−/−}* (*n*=12) animals. **b,**
Schematic describing ambient temperature changes throughout experiment and the duration
of measurement intervals. **c,** Indirect calorimetry (TSE Systems, PhenoMaster® Cages)
measurements of energy expenditure in adult *Opn5^{+/+}* (gray trace, *n*=15) and *Opn5^{−/−}* (blue
trace, *n*=9) animals at ambient temperatures of 22°C, 16°C, 10°C, and 28°C. **d,** Mass-energy
relationships of data in (**c**) represented as generalized linear models. **e,** Respiratory exchange

ratio (RER=VCO$_2$/VO$_2$) obtained from the same animals. **f,** Spontaneous locomotor activity (XY) monitoring was performed via infrared beam breaks. **g,** 24h average food consumption from *Opn5*$^{+/+}$ (gray bars, *n*=11) and *Opn5*$^{-/-}$ (blue bars, *n*=7) animals at each ambient temperature. Mice exhibiting 'food grinding' behavior were excluded from the analysis. **h,** 24h average water consumption from *Opn5*$^{+/+}$ (gray bars, *n*=14) and *Opn5*$^{-/-}$ (blue bars, *n*=9) animals at each temperature. *p* values are from (**a**) two-tailed Student's *t*-tests, (**c, e, f**) 1-way repeated measures ANOVA across 6h time interval, (**d**) two-way ANCOVA with body mass as covariate, and (**g, h**) ANOVA with Holm-Sîdak corrected multiple comparisons. Data in (**c, e, f**) show a 24h period of mean ± s.e.m. data for both genotypes during lights on (6AM – 6PM, yellow shaded region) followed by lights off (6PM – 6AM, gray shaded region). Data in (**a, g, h**) are represented as mean ± s.e.m.
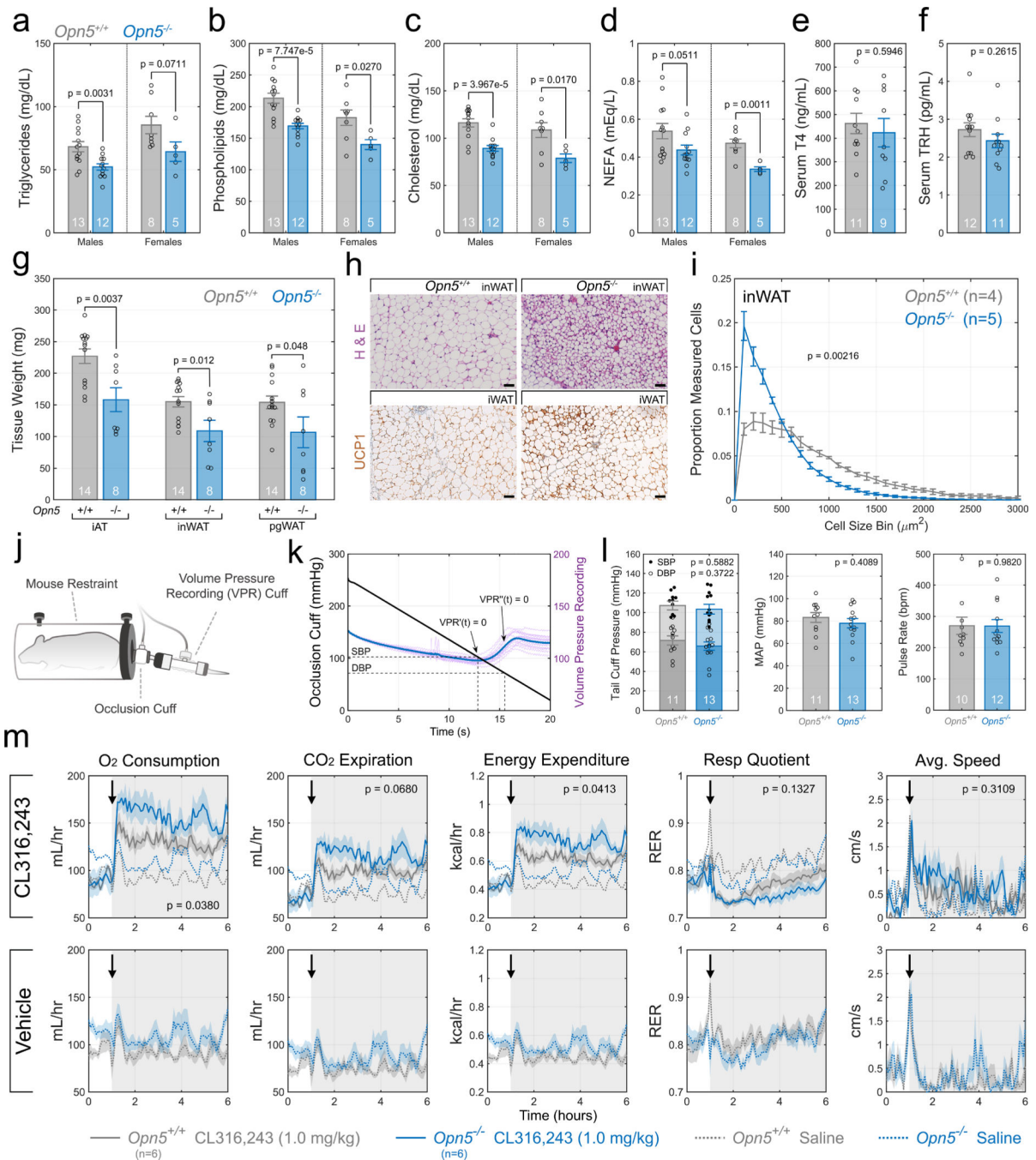
**Extended Data Fig. 6 |. OPN5 regulates thermogenesis and lipid metabolism, but not thyroid and cardiovascular activity.**

**a-d,** Serum lipid quantifications from male ($n$=13 $Opn5^{+/+}$, $n$=12 $Opn5^{-/-}$) and female ($n$=8 $Opn5^{+/+}$, $n$=5 $Opn5^{-/-}$) mice for triglycerides (**a**), phospholipids (**b**), cholesterol (**c**), and non-esterified fatty acids (NEFA) (**d**). **e,** Serum thyroxine (T4) from male $Opn5^{+/+}$ ($n$=11) and $Opn5^{-/-}$ ($n$=9) mice. **f,** Serum thyrotropin-releasing hormone (TRH) from male $Opn5^{+/+}$ ($n$=12) and $Opn5^{-/-}$ ($n$=11) mice. **g,** Adipose depot weight (mg) comparison between male $Opn5^{+/+}$ ($n$=14) and $Opn5^{-/-}$ ($n$=8) mice. iAT, interscapular adipose tissue; inWAT, inguinal

white adipose tissue; pgWAT, perigonadal white adipose tissue. **h,** Representative images highlighting inWAT cell size (H&E) and iWAT UCP1 (IHC) from *Opn5^{+/+}* and *Opn5^{-/-}* animals. Scale bars, 50 μm. **i,** Quantification of inWAT cell size for *Opn5^{+/+}* (*n*=4) and *Opn5^{-/-}* (*n*=5) mice. **j,** Schematic representation of mouse blood pressure recording system. Animals are movement-restricted in a mouse restraint and the tail is fitted proximally with an occlusion cuff and distally with a volume pressure recording (VPR) cuff. **k,** Example trial from tail blood pressure recording. Data are represented as line graphs for occlusion cuff pressure (mmHg; left y-axis) and VPR cuff pressure (mmHg; right y-axis). **l,** Quantification of blood pressure (SBP, systolic blood pressure; DBP, diastolic blood pressure), mean arterial pressure (MAP), and pulse rate (bpm) from *Opn5^{+/+}* (*n*=10–11) and *Opn5^{-/-}* (*n*=12–13) mice. **m,** Indirect calorimetry and locomotion from *Opn5^{+/+}* (*n*=6, gray trace) and *Opn5^{-/-}* (*n*=6, blue trace) mice treated with 1.0 mg/kg β$_3$ adrenergic receptor agonist CL-316,243 (solid line) or vehicle control (saline, dotted line). Intraperitoneal injection of agonist or saline was performed at the 1 hour time point (indicated by arrow). All data are mean ± s.e.m. *p* values are from (**a-g, l**) two-tailed Student's *t*-test, (**i, m**) 1-way repeated measures ANOVA.
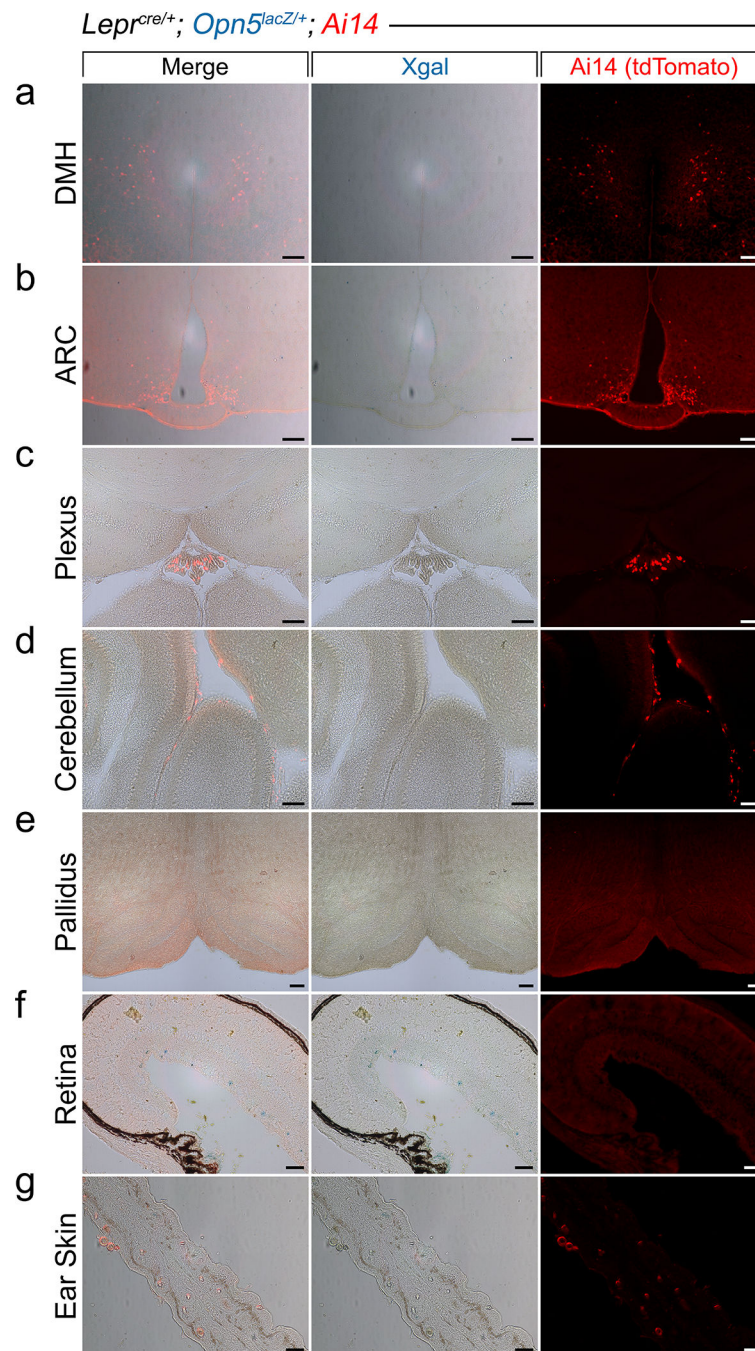
**Extended Data Fig. 7 |. Overlap of *Lepr* and *Opn5* expression is limited to the POA.**
**a-g,** *Lepr*-lineage and *Opn5* expression survey across multiple tissues (*n*=3 mice). Representative images of tdTomato (*Lepr^cre^; Ai14*) and Xgal (*Opn5^lacZ/+^*) domains from the DMH (**a**), arcuate nucleus (ARC) (**b**), choroid plexus (**c**), cerebellum (**d**), raphe pallidus (**e**), retina (**f**), and ear skin (**g**). Scale bars, 100 μm (**a-e**), 50 μm (**f, g**).
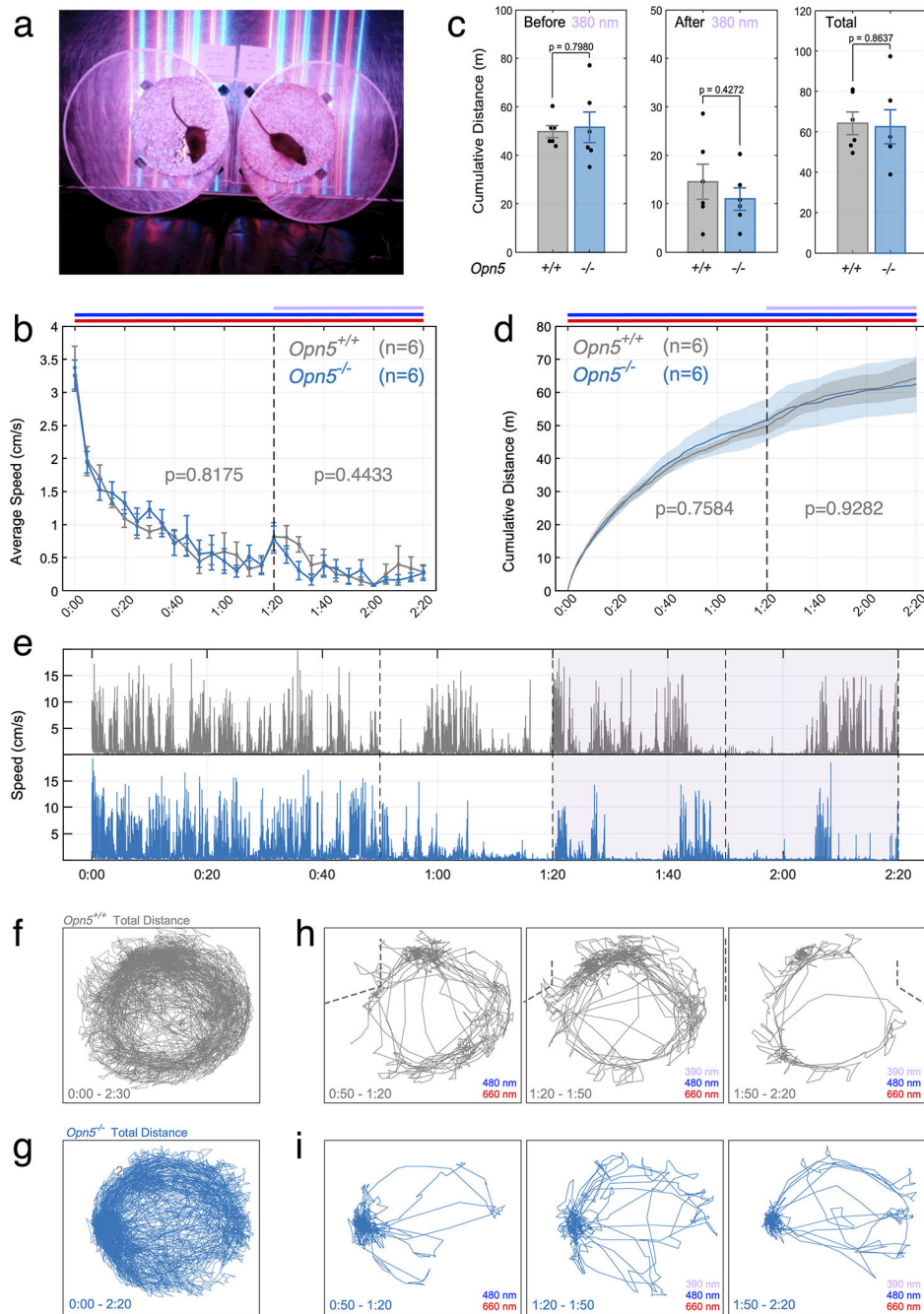
**Extended Data Fig. 8 |. Violet light does not change locomotor behavior in cold exposed mice.**
**a,** Photograph of experimental setup in 4°C. **b,** Average speed in cm/s of 2-month-old male
*Opn5*^{+/+} (gray trace; n=6) and *Opn5*^{−/−} (blue trace; n=6) animals binned in 5 minute
intervals. Violet 380 nm LEDs were switched on after 80 minutes (1:20 mark). **c,**
Cumulative distance in meters traveled by *Opn5*^{+/+} (n=6) and *Opn5*^{−/−} (n=6) animals before
and after violet supplementation, along with total cumulative distance. **d,** Total cumulative
distance plotted across time. **e,** Absolute speed in cm/s of a representative pair (*n*=1 *Opn5*^{+/+}
and *n*=1 *Opn5*^{−/−}) of animals. **f, g,** Representative mouse locomotion trace (centroid-based

motion tracking) of the *Opn5*^{+/+} (**f**) and *Opn5*^{−/−} (**g**) mouse from (**e**). **h, i,** Selective locomotion traces in 30 minute bins ranging from 0:50 – 1:20, 1:20 – 1:50, and 1:50 – 2:20, for the *Opn5*^{+/+} (**h**) and *Opn5*^{−/−} (**i**) experimental pair of animals from (**e**). *p* values are from (**b, d**) 1-way repeated measures ANOVA, and (log *p* value graphs from **b** and **d**), (**c**) two-tailed Student's *t*-test. Data in (**b-d**) are represented as mean ± s.e.m.
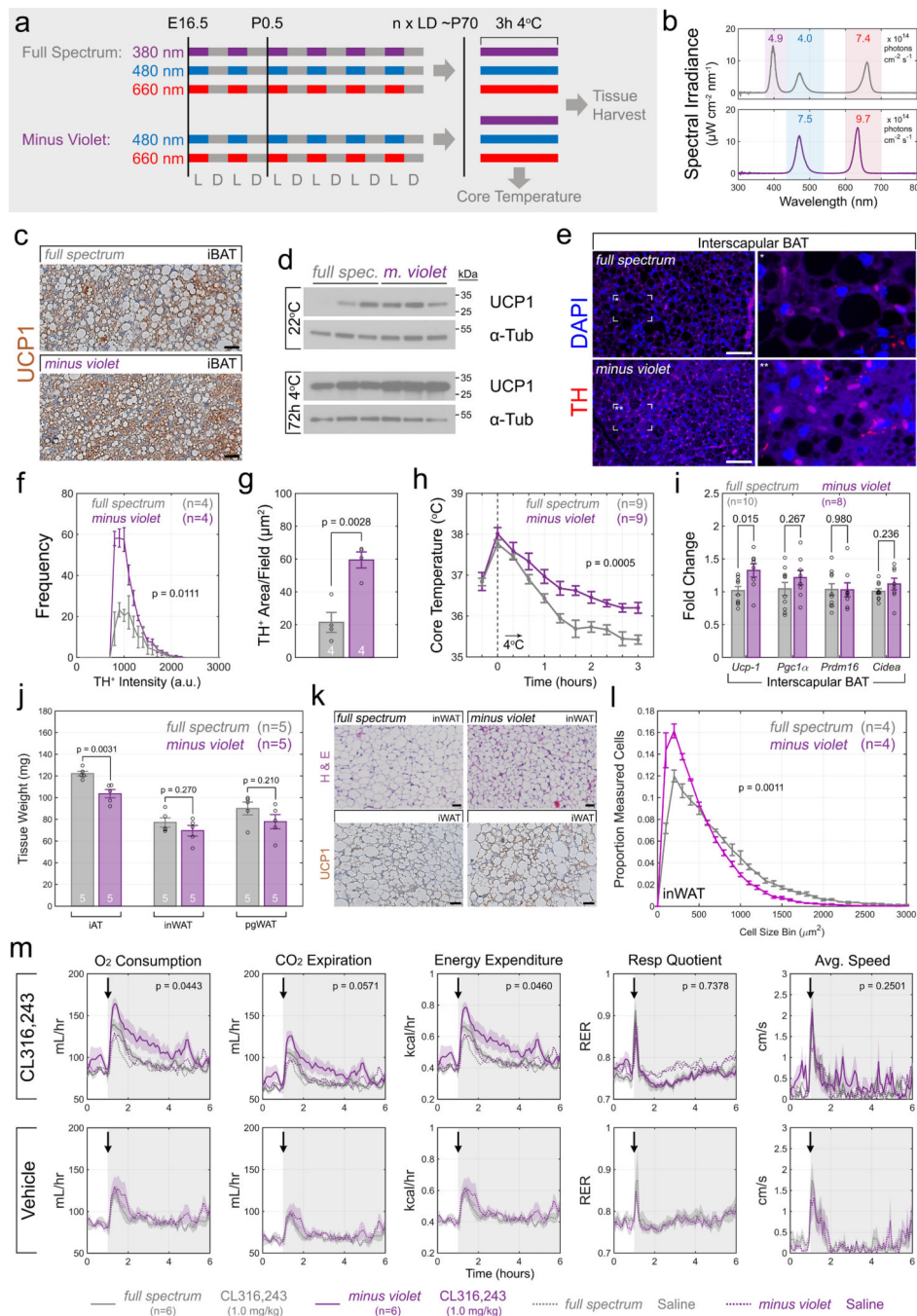


**Extended Data Fig. 9 |. Violet light deprivation alters BAT innervation and sensitivity to SNS input.**

**a,** Lighting protocol used to generate 'full spectrum' and 'minus violet' mice. **b,** Spectral quality of lighting used in 'full spectrum' (top) and 'minus violet' (bottom) housing. Colored boxes indicate wavelength bounds used to estimate flux (photons cm$^{-2}$s$^{-1}$). **c,** UCP1 IHC of 'full spectrum' (top) and 'minus violet' (bottom) mice. **d,** Immunoblots of UCP1 at baseline (22°C) and following 72 hour cold adaptation (72h 4°C) between 'full spectrum' ($n$=3) and 'minus violet' ($n$=3) mice. **e-g,** Representative images (**e**) of TH+ (tyrosine hydroxylase) innervation of BAT used for quantification represented in (**f**) and (**g**). **h,** Core temperature assessment (rectal) of 'full spectrum' and 'minus violet' mice during a 3h cold challenge. **i,** QPCR of thermogenesis genes (*Ucp1, Pgc1a, Prdm16, Cidea*) in iBAT from the mice used in (**h**). **j,** Adipose depot weight (mg) comparison between 'full spectrum' ($n$=5) and 'minus violet' ($n$=5) mice. iAT, interscapular adipose tissue; inWAT, inguinal white adipose tissue; pgWAT, perigonadal white adipose tissue. **k,** Representative images highlighting inWAT cell size (H&E) and iWAT UCP1 (IHC). **l,** Quantification of inWAT cell size H&E images for 'full spectrum' ($n$=4) and 'minus violet' ($n$=4) groups. **m,** Indirect calorimetry from 'full spectrum' ($n$=6, gray trace) and 'minus violet' ($n$=6, purple trace) mice treated with 1.0 mg/kg β$_3$ adrenergic receptor agonist CL-316,243 (solid line) or vehicle (saline, dotted line). Administration of agonist or saline was performed at the 1 hour time point (indicated by arrow). Data are mean ± s.e.m. $p$ values are from (**f, h, l, m**) 1-way repeated measures ANOVA, (**i**) ANOVA with Tukey post-hoc analysis, and (**g, j**) two-tailed Student's $t$-test. Scale bars, 50 μm (**c**), (**e**), and (**k**).
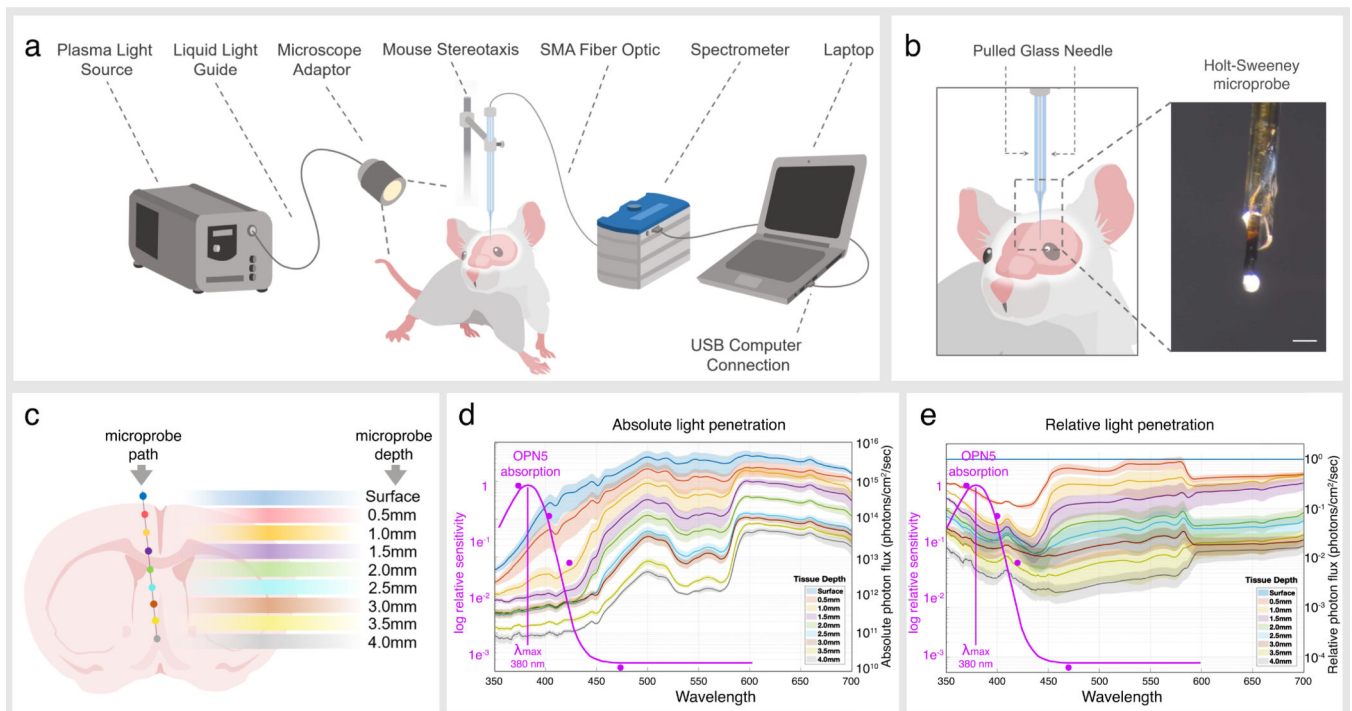


**Extended Data Fig. 10 |. Measurement of photon flux within the POA.**
**a,** Schematic of experimental setup for measuring intra-cranial flux as described in Methods. **b,** Holt-Sweeney microprobe (scale bar, 100 μm) consisting of a pulled optic fiber with an attached transparent spherical diffusing tip. **c,** Measurement depths and probe path within

cranium. **d,** Absolute photon flux within mouse cranium with OPN5 action spectrum superimposed (adapted from[2] with data points from[4]). Upper blue trace represents surface flux and, at the $\lambda_{max}$ of OPN5, is about $3.4 \times 10^{13}$ photons $cm^{-2}s^{-1}$. At the maximum 4.0 mm depth (gray trace), the flux at the $\lambda_{max}$ of OPN5 is approximately $9.5 \times 10^{10}$ photons $cm^{-2}s^{-1}$. **e,** Relative photon flux normalized to surface measurements. Each trace is expressed as mean $\pm$ s.e.m. from $n$=3 mice.

## Supplementary Material

Refer to Web version on PubMed Central for supplementary material.

## Acknowledgements

## References

1. Tarttelin EE, Bellingham J, Hankins MW, Foster RG & Lucas RJ Neuropsin (Opn5): A novel opsin identified in mammalian neural tissue. FEBS Lett. 554, 410–416 (2003). [PubMed: 14623103]

2. Kojima D et al. UV-sensitive photoreceptor protein OPN5 in humans and mice. PLoS One 6, e26388 (2011). [PubMed: 22043319]

3. Buhr ED et al. Neuropsin (OPN5)-mediated photoentrainment of local circadian oscillators in mammalian retina and cornea. Proc. Natl. Acad. Sci. U. S. A 112, 13093–13098 (2015). [PubMed: 26392540]

4. Buhr ED, Vemaraju S, Diaz N, Lang RA & Van Gelder RN Neuropsin (OPN5) Mediates Local Light-Dependent Induction of Circadian Clock Genes and Circadian Photoentrainment in Exposed Murine Skin. Curr. Biol 29, 3478–3487.e4 (2019). [PubMed: 31607531]

5. Yamashita T et al. Evolution of mammalian Opn5 as a specialized UV-absorbing pigment by a single amino acid mutation. J. Biol. Chem 289, 3991–4000 (2014). [PubMed: 24403072]

6. Whitmore D, Foulkes NS & Sassone-Corsi P Light acts directly on organs and cells in culture to set the vertebrate circadian clock. Nature 404, 87–91 (2000). [PubMed: 10716448]

7. Nayak G et al. Adaptive Thermogenesis in Mice Is Enhanced by Opsin 3-Dependent Adipocyte Light Sensing. Cell Rep. 30, 672–686.e8 (2020). [PubMed: 31968245]

8. Sikka G et al. Melanopsin mediates light-dependent relaxation in blood vessels. Proc. Natl. Acad. Sci. U. S. A 111, 17977–17982 (2014). [PubMed: 25404319]

9. Yim PD et al. Activation of an Endogenous Opsin 3 Light Receptor Mediates Photo-Relaxation of Pre-Contracting Late Gestation Human Uterine Smooth Muscle Ex Vivo. Reprod. Sci (2020). doi:10.1007/s43032-020-00180-z

10. Panda S et al. Melanopsin (Opn4) requirement for normal light-induced circadian phase shifting. Science (80-. ). 298, 2213–2216 (2002).

11. Lucas RJ et al. Diminished pupillary light reflex at high irradiances in melanopsin-knockout mice. Science (80-. ). 299, 245–247 (2003).

12. Rao S et al. A direct and melanopsin-dependent fetal light response regulates mouse eye development. Nature 494, 243–246 (2013). [PubMed: 23334418]

13. Fernandez DC et al. Light Affects Mood and Learning through Distinct Retina-Brain Pathways. Cell 175, 71–84.e18 (2018). [PubMed: 30173913]

14. Nakane Y et al. A mammalian neural tissue opsin (Opsin 5) is a deep brain photoreceptor in birds. Proc. Natl. Acad. Sci. U. S. A 107, 15264–15268 (2010). [PubMed: 20679218]

15. Sato M et al. Cell-autonomous light sensitivity via Opsin3 regulates fuel utilization in brown adipocytes. PLoS Biol. 18, e3000630 (2020). [PubMed: 32040503]

16. Tan CL & Knight ZA Regulation of Body Temperature by the Nervous System. Neuron 98, 31–48 (2018). [PubMed: 29621489]

17. Morrison SF, Madden CJ & Tupone D Central neural regulation of brown adipose tissue thermogenesis and energy expenditure. Cell Metabolism 19, 741–756 (2014). [PubMed: 24630813]

18. Tan CL et al. Warm-Sensitive Neurons that Control Body Temperature. Cell 167, 47–59.e15 (2016). [PubMed: 27616062]

19. Song K et al. The TRPM2 channel is a hypothalamic heat sensor that limits fever and can drive hypothermia. Science (80-. ). (2016). doi:10.1126/science.aaf7537

20. Takatoh J et al. New Modules Are Added to Vibrissal Premotor Circuitry with the Emergence of Exploratory Whisking. Neuron 77, 346–360 (2013). [PubMed: 23352170]

21. Nguyen MTT et al. An opsin 5–dopamine pathway mediates light-dependent vascular development in the eye. Nat. Cell Biol 21, 420–429 (2019). [PubMed: 30936473]

22. Wong KY A retinal ganglion cell that can signal irradiance continuously for 10 hours. J. Neurosci 32, 11478–11485 (2012). [PubMed: 22895730]

23. Muntean BS et al. Interrogating the Spatiotemporal Landscape of Neuromodulatory GPCR Signaling by Real-Time Imaging of cAMP in Intact Neurons and Circuits. Cell Rep. (2018). doi:10.1016/j.celrep.2017.12.022

24. Fernandes AM et al. Deep brain photoreceptors control light-seeking behavior in zebrafish larvae. Curr. Biol 22, 2042–2047 (2012). [PubMed: 23000151]

25. Yu S et al. Glutamatergic preoptic area neurons that express leptin receptors drive temperature-dependent body weight homeostasis. J. Neurosci 36, 5034–5046 (2016). [PubMed: 27147656]

26. Machado NLS, Bandaru SS, Abbott SBG & Saper CB EP3R-Expressing Glutamatergic Preoptic Neurons Mediate Inflammatory Fever. J. Neurosci 40, 2573–2588 (2020). [PubMed: 32079648]

27. Moffitt JR et al. Molecular, spatial, and functional single-cell profiling of the hypothalamic preoptic region. Science (80-. ). 362, (2018).

28. Boland MR, Shahn Z, Madigan D, Hripcsak G & Tatonetti NP Birth month affects lifetime disease risk: A phenome-wide method. J. Am. Med. Informatics Assoc 22, 1042–1053 (2015).

29. Kahn HS et al. Association of type 1 diabetes with month of birth among U.S. youth: The SEARCH for diabetes in youth study. Diabetes Care 32, 2010–2015 (2009). [PubMed: 19675199]

30. Holt AL, Vahidinia S, Gagnon YL, Morse DE & Sweeney AM Photosymbiotic giant clams are transformers of solar flux. J. R. Soc. Interface 11, 20140678 (2014). [PubMed: 25401182]
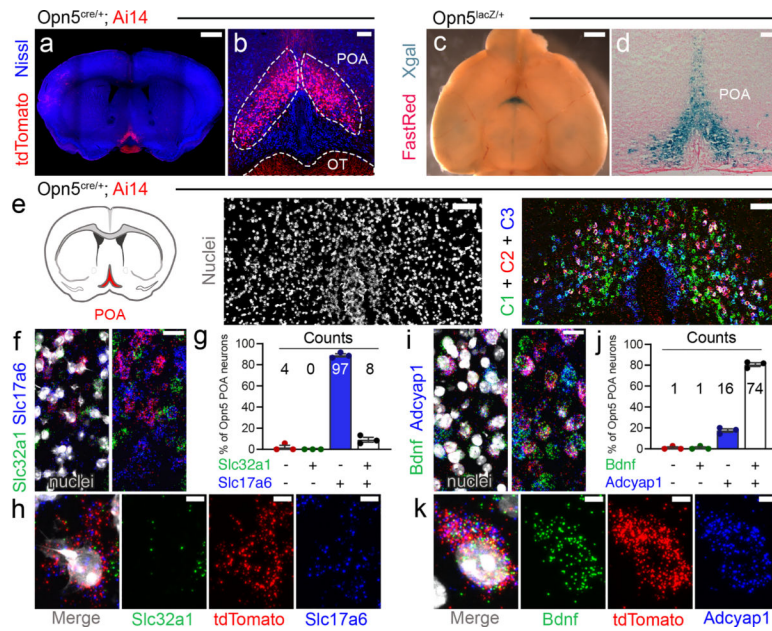
**Fig. 1 |.** *Opn5* **is expressed in a population of hypothalamic POA neurons that receive input from thermoregulatory nuclei.**

**a, b,** Coronal brain section (P21 *Opn5*^cre/+^; *Ai14*) showing *Opn5* (tdTomato, red) restricted to the preoptic area (POA). Nissl labeling is blue. Red labeling in optic tracts (OT) are axons from *Opn5* retinal ganglion cells. **c, d,** Xgal labeling (P10 *Opn5*^lacZ/+^) in (**c**) whole brain, ventral view and (**d**) coronal section through POA. **e,** M-FISH (see Methods) region schematic and low magnification images of nuclear (DAPI, greyscale) and three-colour probe labeling. **f, g,** Representative images of POA neurons (**f**) probed for *tdTomato* (*Opn5*^cre^; *Ai14*, red), *Slc32a1* (*Vgat*, green), and *Slc17a6* (*Vglut2*, blue) with (**g**) quantification of overlap (*n*=3, 109 cells). **h,** Representative tdTomato+ cell from (**f**). **i, j,** As in (**f, g**) but for *tdTomato* (*Opn5*^cre^; *Ai14*, red), *Bdnf* (green), and *Adcyap1* (encoding PACAP, blue) with (**j**) quantification (*n*=3; 92 cells). **k,** Representative tdTomato+ cell from (**i**). **l,** Schematic of the mouse genetics used for rabies viral tracing. **m,** Experimental timeline for POA-tracing, and primary infected neurons (yellow). **n-w,** Traced neurons (red) located in the paraventricular nucleus; PVN (**o, p**), supraoptic nucleus; SON (**o, q**), dorsomedial hypothalamus; DMH (**r, s**), lateral parabrachial; LBP (**t, u**), and raphe pallidus; RPa (**v, w**). Green regions in (**o, q**) are optic tracts with axons from *Opn5* retinal ganglion cells. **x,** Schematic representation of nuclei presynaptic to *Opn5* POA neurons. Scale bars, 5 μm (**h, k**), 20 μm (**f, i**), 75 μm (**e, m**), 100 μm (**b, p, q, s, w**), 200 μm (**o, u**), 1 mm (**a**). 2Cb, lobule 2 of cerebellar vermis. Data in **g**, **i** are mean ± s.e.m.
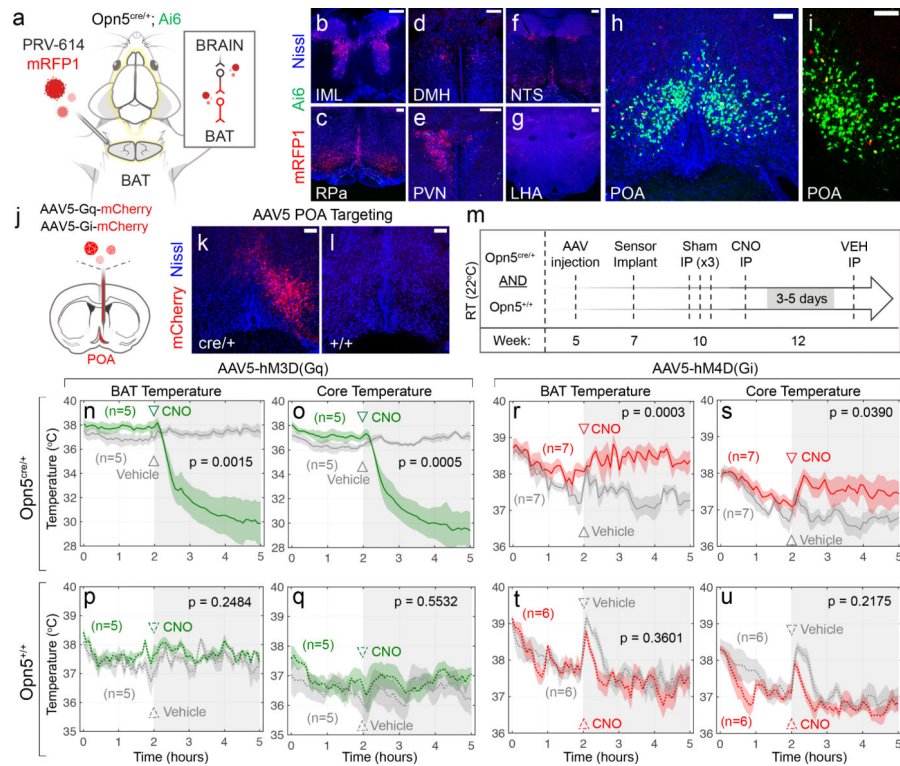
**Fig. 2 |. *Opn5* POA neurons regulate BAT thermogenesis.**
**a,** Pseudorabies virus (PRV-mRFP1) injection into the BAT of P60 *Opn5^cre/+^; Ai6* mice. **b-i,** Representative images of PRV-infected (red) regions including the intermediolateral nucleus (IML) of the spinal cord (**b**), RPa (**c**), DMH (**d**), PVN (**e**), nucleus tractus solitarius (NST) (**f**), lateral hypothalamic area (LHA) (**g**), and *Opn5; Ai6* (green) POA neurons (**h, i**). **j,** Schematic of DREADD virus delivery into the POA of *Opn5^cre/+^* or *Opn5^+/+^* animals. **k, l,** IF showing AAV-infected POA neurons in *Opn5^cre/+^* (**k**) and lack thereof in *Opn5^+/+^* (**l**). **m,** Experimental timeline. **n-u,** Chemogenetic manipulation of *Opn5* POA neurons. CNO or vehicle (saline) injected at hour 2 (open arrowhead). CNO-mediated activation of *Opn5* POA neurons with Gq DREADD decreases BAT and core temperature in *Opn5^cre/+^* animals (**n, o**) but not in *Opn5^+/+^* controls (**p, q**). CNO-mediated inhibition of *Opn5* POA neurons with Gi DREADD increases BAT and core temperature in *Opn5^cre/+^* animals (**r, s**) but not in controls (**t, u**). Scale bars, 100 μm. Data in **n-u** are mean ± s.e.m. All *p* values represent 1-way repeated measures ANOVA.
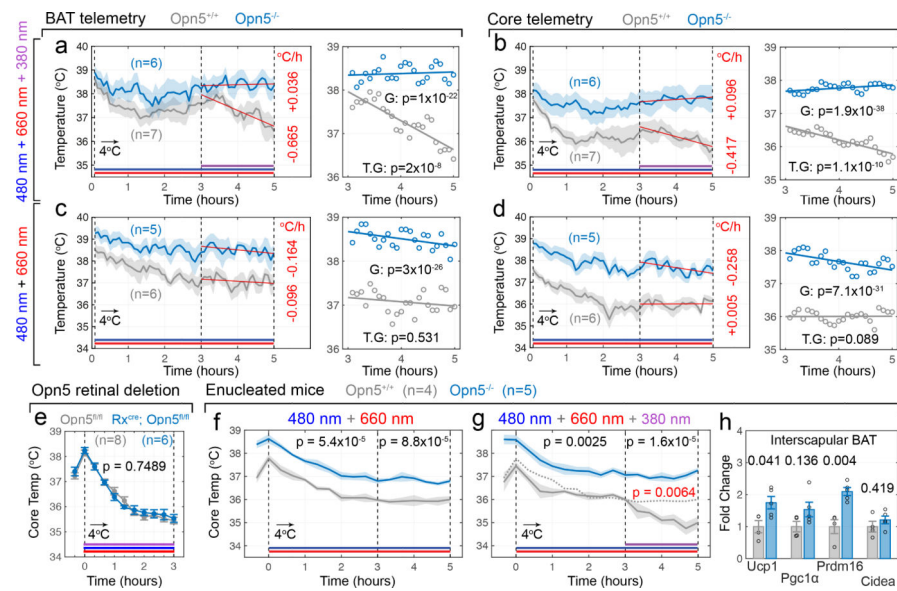
**Fig. 3 |. Violet light acutely suppresses BAT thermogenesis.**

**a-d,** BAT and core telemetry recordings during 5 hour 4°C exposure with lighting wavelength modulation. All mice received 480 nm and 660 nm light exposure (see Methods). At the 3 hour mark (dotted line), *Opn5^{+/+}* or *Opn5^{−/−}* animals were either supplemented with 380 nm light (**a, b**) or remained in 480 nm + 660 nm (**c, d**). BAT and core temperature trajectories during light modulation (hours 3–5) were calculated via linear regression and the rate of temperature change reported as °C/h. **e,** Core temperature assessment (rectal) of *Opn5^{fl/fl}* and *Rx^{cre}; Opn5^{fl/fl}* mice during 3h cold challenge in 380 nm + 480 nm + 660 nm lighting. **f, g,** Core temperature assessment in enucleated *Opn5^{+/+}* (*n*=4) and *Opn5^{−/−}* (*n*=5) mice under 480 nm + 660 nm illumination (**f**) or supplemented with 380 nm violet light (**g**) at hour 3 (dotted line). Dotted trace in (**g**) represents wild-type average trace from (**f**). **h,** iBAT QPCR of thermogenesis genes (*Ucp1, Pgc1α, Prdm16, Cidea*) following 5h cold exposure in mice from (**g**). Data are mean ± s.e.m. *p* values are from (**a-d**) 1-way ANCOVA with time as covariate, (**e-g**) 1-way repeated measures ANOVA, (**h**) ANOVA with Tukey post-hoc analysis.
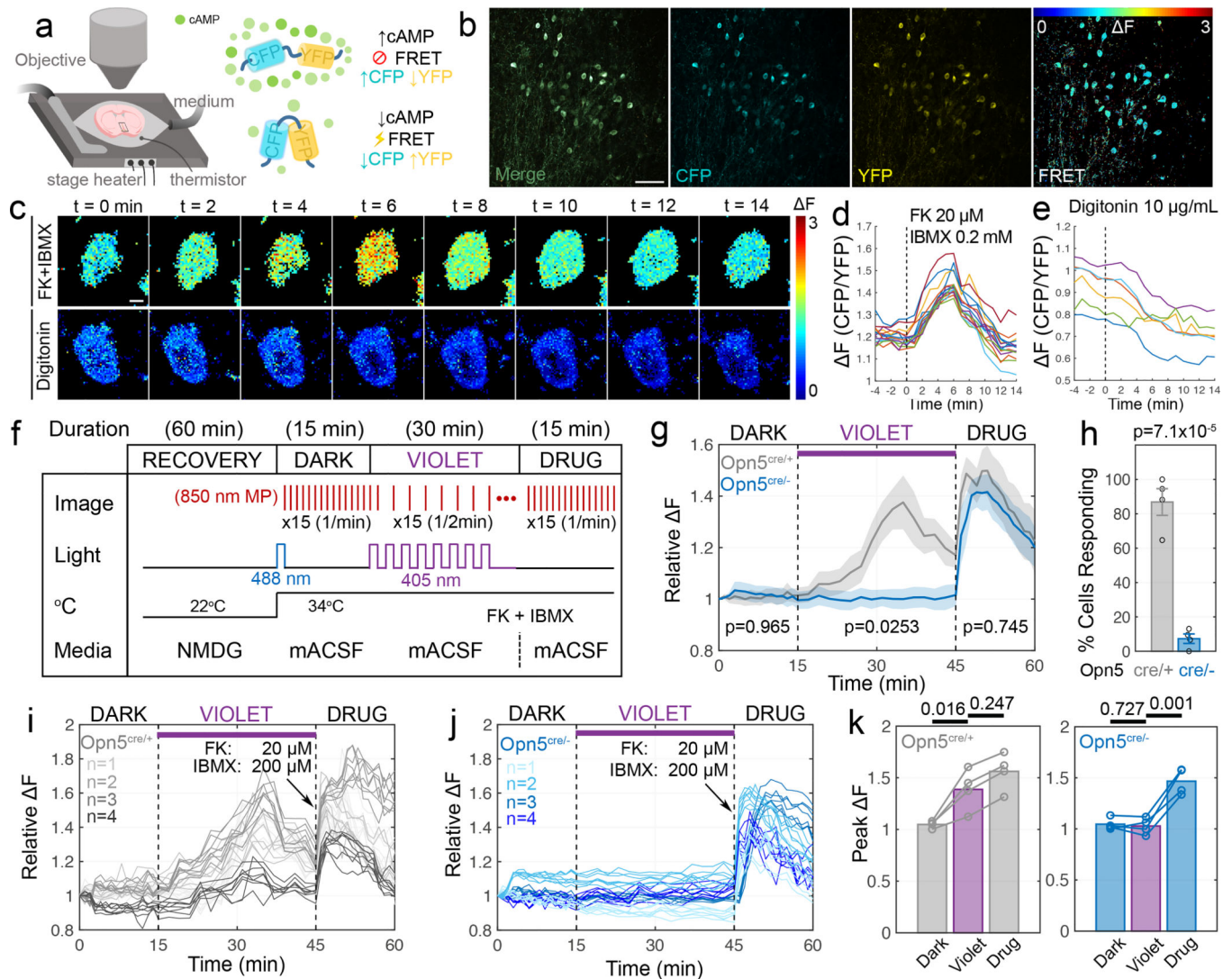
**Fig 4. |. *Opn5* POA neurons respond to violet light *ex vivo*.**
**a,** Schematic depicting two-photon assessment of cAMP biosensor FRET activity in POA
slices from *Opn5^cre^; CAMPER* mice. **b,** CFP, YFP, and FRET images (expressed as
 F=CFP/YFP ratio). **c,** Time course  F images following response to forskolin (FK, 20 μM)
and IBMX (200 μM) (top row) or digitonin (10 μg/mL) (bottom row). **d, e,** Individual traces
from FK + IBMX (**d**, *n*=15 cells) or digitonin (**e**, *n*=6 cells) treated slices. **f,** Experimental
timeline for testing violet responses of *Opn5* neurons in POA slices as described in Methods.
**g,** Relative  F plots for *Opn5^cre/+^* (gray trace, *n*=4) and *Opn5^cre/-^* (blue trace, *n*=4) animals.
**h,** Percent of cells responding to violet light (average relative  F > 1.1 between t=15 and
t=45) for both groups. **i, j,** Individual traces from each biological replicate (*n*=6–8 cells per
animal, 4 animals per genotype) from experiments in (**g**). **k,** Peak  F from dark, violet
stimulation, and drug phases between *Opn5^cre/+^* and *Opn5^cre/-^* animals. Data in **g, h, k** are
presented as mean ± s.e.m. *p* values are from (**g**) 1-way repeated measures ANOVA, (**h, k**)
two-tailed Student's *t*-test. Scale bars, 10 μm (**c**), 100 μm (**b**).